Acta Pharmaceutica Sinica B 2025;15(4):2039−2058

Chinese Pharmaceutical Association
Institute of Materia Medica, Chinese Academy of Medical Sciences

Acta Pharmaceutica Sinica B

www.elsevier.com/locate/apsb
www.sciencedirect.com

ORIGINAL ARTICLE

p52-ZER6/DAZAP1 axis promotes ferroptosis resistance and colorectal cancer progression *via* regulating *SLC7A11* mRNA stabilization

Li Qiu[a,b], Wenfang Li[a,b], Lei Zhang[a,b], Xia Zhang[a,b], Hezhao Zhao[c], Makoto Miyagishi[d], Shourong Wu[a,b,*], Vivi Kasim[a,b,*]

[a]*Key Laboratory of Biorheological Science and Technology, Ministry of Education, College of Bioengineering, Chongqing University, Chongqing 400044, China*
[b]*The 111 Project Laboratory of Biomechanics and Tissue Repair, College of Bioengineering, Chongqing University, Chongqing 400044, China*
[c]*Department of Gastrointestinal Surgery, Chongqing University Cancer Hospital, Chongqing University, Chongqing 400030, China*
[d]*Life Science Innovation, School of Integrative and Global Majors, University of Tsukuba, Tsukuba, Ibaraki 305-0006, Japan*

Received 16 July 2024; received in revised form 27 September 2024; accepted 5 November 2024

KEY WORDS

Tumor cell ferroptosis;
mRNA stabilization;
RNA binding protein;
Zinc-finger protein;
ZER6;
p52-ZER6;
DAZAP1;
SLC7A11

Abstract Resistance to ferroptosis, a form of regulated cell death caused by disruptions in iron ion and intracellular redox homeostasis, is closely related to tumorigenesis and tumor drug resistance; therefore, targeting ferroptosis-related pathways has garnered attention as a potential antitumor therapeutic strategy. However, the molecular mechanisms underlying ferroptosis resistance in tumor cells remain unknown. Zinc-finger estrogen receptor interaction clone 6 (ZER6) consists of two isoforms with distinct N-termini, p52-ZER6 and p71-ZER6. ZER6 is upregulated in tumors and promotes tumorigenic potential; however, whether ZER6 is involved in tumor cell ferroptosis resistance remains unknown. Herein, we identified p52-ZER6 as a novel regulator of tumor cell ferroptosis resistance. p52-ZER6 promotes the transcriptional activity of *DAZAP1*, an RNA-binding protein. DAZAP1, in turn, enhances the stability of *SLC7A11* mRNA by binding to its 3′-UTR region, thereby increasing SLC7A11 expression and cellular glutathione levels. This subsequently reduces lipid peroxide accumulation and enhances tumor cell ferroptosis resistance, eventually promoting tumorigenic potential. These findings reveal a new

*Corresponding authors.
E-mail addresses: shourongwu@cqu.edu.cn (Shourong Wu), vivikasim@cqu.edu.cn (Vivi Kasim).

Peer review under the responsibility of Chinese Pharmaceutical Association and Institute of Materia Medica, Chinese Academy of Medical Sciences.

https://doi.org/10.1016/j.apsb.2025.02.013

function of p52-ZER6 in regulating *SLC7A11* mRNA stability *via* DAZAP1, ultimately leading to ferroptosis resistance and tumorigenic potential. Additionally, we also suggest targeting p52-ZER6 as a potential strategy to promote the efficacy of ferroptosis-based antitumor therapies.

1. Introduction

Cell death resistance is one of the fourteen hallmarks of cancer[1]. According to cell morphology and context, as well as the triggering stimuli, cell death can be classified as uncontrolled, accidental cell death and active, orderly processed, regulated cell death (RCD)[2-4]. RCD, which mainly includes apoptosis, autophagy, necroptosis, ferroptosis, and pyroptosis, can function as a defense mechanism against malignancy; therefore, abnormalities in RCD can lead to tumor initiation, progression, and drug resistance[5]. In the early stages of cancer, mutations in tumor suppressor genes, such as *BRCA1/2* and *p53* can disrupt RCD pathways, thereby accelerating tumor initiation and promoting antitumor therapeutic resistance[6,7]. With tumor development, cell death resistance supports sustained cell growth by overcoming the harsh tumor microenvironment, which becomes increasingly deficient in oxygen and nutrients[8,9]. In later stages of cancer, cell death resistance helps tumor cells to survive and metastasize by circumventing the limitation of proliferative signaling at metastatic sites[10]. Hence, cell death resistance is crucial for every step of tumorigenesis.

Ferroptosis is an iron-dependent form of RCD triggered by the disruption of iron ion and redox homeostasis[11,12]. Ferroptosis can occur *via* three main pathways: an imbalance in iron ion homeostasis, which results in the accumulation of lipid peroxides; impaired synthesis of glutathione (GSH), a cellular reductant that reduces lipid peroxides; and aberrant expression of glutathione peroxidase 4 (GPX4), an enzyme that reduces lipid peroxides using GSH[13-15]. Recent studies have shown that ferroptosis plays crucial roles in tumor progression, drug resistance, and poor patient prognosis[16,17]. Tumor cells often develop an iron dependency, leading to an increase in reactive oxygen species (ROS) levels during tumorigenesis, and therefore are prone to ferroptosis induction[18,19]. Accumulating evidence demonstrates that inducing ferroptosis may be a potential antitumor therapeutic strategy, as even tumor cells that are resistant to conventional therapy may be sensitive to ferroptosis[20-22]. However, the molecular mechanisms that enable tumor cells to resist ferroptosis remain largely unexplored.

Zinc-finger estrogen receptor interaction clone 6 (ZER6, also known as ZNF398) is a member of the Krüppel C2H2-type zinc-finger protein family. ZER6 comprises two isoforms with different N-termini: p52-ZER6 and p71-ZER6. While the N-terminus of p71-ZER6 has a full-length Krüppel-associated box (KRAB) and a HTLV-I U5RE-binding protein 1 (HUB-1) domains, that of p52-ZER6 has a truncated KRAB domain with only 30 C-terminal amino acids[23,24]. Recent studies have revealed the tumorigenic functions of p52-ZER6, as it can promote cell cycle progression, tumor cell proliferation, and the pentose phosphate pathway[25-27]. However, studies on the biological and pathological functions of ZER6 remain limited, and whether this protein is involved in ferroptosis resistance in tumor cells remains unknown.

Herein, using transcriptome analysis, we identified ZER6 as a novel ferroptosis regulator. Systematic investigations further revealed that this function is specific to the p52-ZER6 isoform, which improves solute carrier family 7 member 11 (*SLC7A11*) mRNA stability by promoting the transcriptional activity of the gene encoding deleted in azoospermia associated protein 1 (DAZAP1), an RNA-binding protein (RBP) crucial for regulating mRNA stability[28,29]. This, in turn, enhances tumor cell ferroptosis resistance and subsequently, tumorigenic potential. These findings uncover a novel mechanism of tumor cell ferroptosis resistance and provide new insights into the role of p52-ZER6 in maintaining cellular redox homeostasis.

2. Materials and methods

2.1. Vectors construction

Short hairpin RNA (shRNA) expression vectors targeting *ZER6*, *p52-ZER6*, *p71-ZER6*, and *SLC7A11* were constructed as described previously[25,30]. The target sequences were as follows: shZER6-1: 5′-AGC CAG AAT CTG GAC CTA T-3′; shZER6-2: 5′-GTA TTA TGT TCC CCT TCT G-3′; shp52-1: 5′-GAG AGG ACG TAG TCT TGC T-3′; shp52-2: 5′-GAC TGA GAG GCA GCG AGA A-3′; shp71-1: 5′-GGG GAA GGC AGG GCC GGG T-3′; shp71-2: 5′-GCT TGG AGC CGG GCG CGG T-3′; shSLC7A11-1: 5′-GGA ACA ACT ATA AAG AAA T-3′; shSLC7A11-2: 5′-GGT CAA ACG CAG AAC TTT A-3′. Vectors overexpressing *p52-ZER6*, *p71-ZER6*, and *SLC7A11* (pcp52-ZER6, pcp71-ZER6, and pcSLC7A11, respectively), as well as vectors overexpressing *p52-ZER6* with full-length KRAB domain (pcFLAGp52^{K}), *p52-ZER6* with full-length KRAB and HUB-1 domains (pcFLAGp52^{KH}), and *p52-ZER6* without tKRAB domain (pcFLAGp52^{tKdel}) were constructed as described previously[25,30]. For *DAZAP1* overexpression vector (pcDAZAP1), the coding region of human *DAZAP1* was obtained by reverse-transcribing total RNA extracted from HCT116^{WT} colorectal cancer (CRC) cells using the PrimeScript Reagent Kit with gDNA Eraser (Takara Bio, Dalian, China) and amplifying the corresponding regions using Takara Prime STAR Max DNA Polymerase (Takara Bio, Dalian, China). The amplicon was inserted into the *Bam*HI and *Mlu*I sites of pcEF9-Puro vector bringing puromycin resistance gene[31].

For reporter vector bringing −127 to +1520 region of the *SLC7A11* promoter (SLC7A11-luc), as well as the −1621 to +1239 (DAZAP1-luc1), the −1274 to +1239 (DAZAP1-luc2), the +508 to +1239 (DAZAP1-luc3), the +741 to +1239 (DAZAP1-luc4), and the +867 to +1239 (DAZAP1-luc5) regions of the *DAZAP1* promoter, human genome DNA extracted from HCT116^{WT} cells using Genomic DNA Kit (Tiangen Biotech, Beijing, China) was used as a template for amplifying the corresponding regions using Takara PrimeSTAR Max DNA Polymerase (Takara Bio, Dalian, China). For SLC7A11-luc, the amplicon was then cloned into the *Nhe*I and *Apa*I sites of the pGL4.13 vector (Promega, Madison, WI, USA); while for DAZAP1-lucs, the amplicons were cloned into the *Nhe*I and *Stu*I sites of the pGL4.13

vector. For reporter vectors bringing the *SLC7A11* 5′-UTR (SLC7A11-5′-UTR-luc), *SLC7A11* CDS (SLC7A11-CDS-luc), and *SLC7A11* 3′-UTR (SLC7A11-3′-UTR-luc-1: 1 to 1517; SLC7A11-3′-UTR-luc-2: 1491 to 3353; SLC7A11-3′-UTR-luc-3: 3296 to 4788; SLC7A11-3′-UTR-luc-4: 4735 to 6332; SLC7A11-3′-UTR-luc-5: 6325 to 7789; SLC7A11-3′-UTR-luc-4A: 4728 to 5023; SLC7A11-3′-UTR-luc-4B: 5110 to 6332), the corresponding regions were amplified from human genome DNA as described above, and the amplicons were cloned into the *Xho*I and *Not*I sites of the psiCHECK-2 vector (Promega, Madison, WI, USA). DAZAP1 luciferase reporter vector with mutated ZER6 binding site (DAZAP1-Luc^{mut}) and SLC7A11 luciferase reporter vector with mutated DAZAP1 binding site (SLC7A11-Luc^{mut}) were constructed from DAZAP1-luc4 and SLC7A11-3′UTR-luc-4A, respectively, by mutating the corresponding binding sites using Site-directed Mutagenesis Kit (Beyotime Biotechnology, Shanghai, China).

2.2. Cell lines and cell culture

Wild-type HCT116, LoVo, and HT29 CRC cell lines were purchased from the Cell Bank of Chinese Academy of Sciences (Shanghai, China). *p53-null* HCT116 (HCT116^{p53null}) cell line was kindly provided by Dr. Bert Vogelstein at John Hopkins University School of Medicine. Wild-type HCT116 and HT29 cells were cultured in Dulbecco's modified Eagle's medium (Gibco, Life Technologies, Grand Island, NY, USA); while LoVo and HCT116^{p53null} cells were cultured in F12K Ham's Kaighn's modified medium (Macgene, Beijing, China) and McCoy's 5A medium (Gibco), respectively. All culture media were supplemented with 10% FBS (Biological Industries, Beith Haemek, Israel) and 1% penicillin−streptomycin. All cell lines were verified using short-tandem repeat profiling method and were tested periodically for mycoplasma contamination by using Mycoplasma Detection Kit−Quick Test (Biotool, Houston, TX, USA) routinely every 6 months. Transfection was performed using Lipofectamine 2000 (Invitrogen Life Technologies, Carlsbad, CA, USA) according to the manufacturer's instructions. For gene-silencing and gene-overexpression experiments, cells were seeded in a 6-well plate and transfected with 2 μg of the indicated vector. After 24 h, cells were selected using puromycin (final concentration: 1.0 μg/mL) for 36 h to eliminate untransfected cells.

For establishing cell lines stably expressing indicated shRNA and/or overexpression vectors, HCT116^{WT} or HCT116^{p53null} cells were transfected with corresponding shRNA and/or overexpression vectors. Twenty-four hours later, puromycin selection (final concentration: 1 μg/mL) was for 7 days to eliminate untransfected cells.

For establishing ferroptosis-resistant HCT116 cells (HCT116^{EraR}), cells were seeded in 10 cm-well plates and cultured with medium containing a low-dose Erastin (MedChem Express, Monmouth Junction, NJ, USA; final concentration: 5 μmol/L) for 26 days.

For cell death inhibitor experiments, cells were treated with Ferrostatin-1 (Ferr-1; MedChem Express, Monmouth Junction, NJ; final concentration: 5 μmol/L), 3-methyladenine (3-MA; MedChem Express, Monmouth Junction, NJ, USA; final concentration: 10 μmol/L), Necrosulfonamide (NSA; MedChem Express, Monmouth Junction, NJ, USA; final concentration: 5 μmol/L), Z-VAD-FMK (Z-VAD; APExBIO, Houston, TX, USA; final concentration: 20 μmol/L) and Erastin (MedChem Express, Monmouth Junction, NJ, USA), treating cells with indicated concentrations for indicated times before detection.

2.3. Clinical human CRC specimens

Human CRC specimens were obtained from CRC patients undergoing surgery at Chongqing University Cancer Hospital (Chongqing, China) and stored in the Biological Specimen Bank of Chongqing University Cancer Hospital. Patients did not receive chemotherapy, radiotherapy, or other adjuvant therapies prior to surgery. The specimens were snap-frozen in liquid nitrogen. Prior patient's written informed consents were obtained. The experiments were approved by the Institutional Research Ethics Committee of Chongqing University Cancer Hospital (Permit No. CZLS2021292-A), and conducted in accordance with Declaration of Helsinki.

2.4. Animal experiment

For the *in vivo* tumor study, BALB/c-*nu*/*nu* mice (male, 6-weeks old, body weight: 18−22 g) were purchased from Chongqing Medical University (Chongqing, China). Animal studies were conducted in the Chongqing University Cancer Hospital, and approved by the Laboratory Animal Welfare and Ethics Committee of Chongqing University Cancer Hospital. All animal experiments conformed to the approved Guidelines for the Care and Use of Laboratory Animals of the Chongqing University Cancer Hospital (Permit No. SYXK-2021-0001). All efforts were made to minimize suffering.

For the xenograft experiment, mice were randomly divided into three groups ($n = 6$) and each group was injected subcutaneously with 5×10^6 indicated stable cell lines. Tumor size (V) was evaluated by a caliper every 2 days with reference to Eq. (1):

$$V = a \times b^2/2 \quad (1)$$

where a and b are the major and minor axes of the tumor, respectively. The investigator was blinded to the group allocation and during the assessment.

2.5. RNA sequencing (RNA-seq) and transcriptomic analysis

HCT116^{WT} cells were transfected with shZER6 or control vector (shCon) as described above. RNA extraction and RNA-seq were performed by Novogene Technology Corporation (Beijing, China) using an Illumina HiSeq 2500 instrument (Illumina, San Diego, CA, USA; three repetitive for each group). Raw reads were preprocessed by filtering out rRNA reads, sequencing adapters, short-fragment reads, and other low-quality reads. Tophat v2.1.0 was used to map the clean reads to the human reference genome ensemble GRCh38 (hg38) with two mismatches. After genome mapping, Cufflinks v2.1.1 was run with reference annotations to generate fragments per kilobase per million mapped reads values for known gene models. Differentially expressed genes (DEGs) were identified using Cuffdiff software. The *P*-value significance threshold for DEGs in multiple tests was set based on a false discovery rate ≤ 0.05. The fold-changes were estimated according to the fragments per kilobase per million mapped reads in each sample.

2.6. Transmission electron microscopy

Cells were prepared as described above and fixed with 2.5% glutaraldehyde, washed in 0.1 mol/L phosphate buffer (pH 7.4), and post-fixed with 1% osmium 0.1 mol/L phosphate buffer. Samples were dehydrated in series acetone, infiltrated, and embedded in Epox812 before being cut into ultra-thin sections.

Sections were stained with uranyl acetate and lead citrate prior to being examined using JEM-1400-FLASH transmission electron microscope (JEOL, Tokyo, Japan).

2.7. RNA immunoprecipitation (RIP) assay

Cells were lysed with RIP lysis buffer with protease inhibitor and RNase inhibitor (Beyotime Biotechnology, Shanghai, China). Cell lysates were then incubated with anti-DAZAP1 (Santa Cruz Biotechnology, Santa Cruz, CA, USA) or IgG antibody for 4 h before being immunoprecipitated with protein A/G beads (MCE, Shanghai, China). RNA was extracted with trizol (Invitrogen Life Technologies, Carlsbad, CA, USA) according to the manufacturer's instruction, and reverse transcribed into cDNA using PrimeScript Reagent Kit with gDNA Eraser (Takara Bio, Dalian, China). qRT-PCR was performed using SYBR Premix ExTaq (Takara Bio, Dalian, China). The sequences of the primers used for qRT-PCR are shown in Supporting Information Table S1.

2.8. Biotinylated RNA pull-down assay

DNA fragments containing *T7 RNA polymerase* promoter sequences and sequences correspond to different regions of *SLC7A11* mRNA were amplified using Takara PrimeSTAR Max DNA Polymerase (Takara Bio, Dalian, China) from human genome DNA as described above. The amplicons were then used as templates for *in vitro* transcription using RiboTM RNAmax-T7 (Ribo Bio, Guangzhou, China) to obtain biotinylated RNAs. Cells were lysed with RIP lysis buffer containing protease inhibitor and RNase inhibitor (Beyotime Biotechnology, Shanghai, China), and the cell lysates were incubated with biotinylated RNAs for 4 h at 4 °C. The RNA-protein complexes were then added to streptavidin magnetic beads (MCE, Shanghai, China) overnight at 4 °C, and the precipitants were then analyzed by Western blotting with an anti-DAZAP1 antibody (Santa Cruz Biotechnology, Santa Cruz, CA, USA).

2.9. Chromatin immunoprecipitation (ChIP) assay

ChIP assay was performed using the ChIP assay kit (Beyotime Biotechnology, Shanghai, China) according to the manufacturer's instructions. Briefly, cells were lysed and chromatins were immunoprecipitated using protein A + G agarose/salmon sperm DNA and anti-ZER6 antibody, anti-histone H3 antibody, or normal rabbit IgG. Chromatin was then de-crosslinked for 4 h at 65 °C before being treated with 0.5 mol/L EDTA, 1 mol/L Tris (pH 6.5), and 20 mg/mL proteinase K. Immunoprecipitated chromatin was then subjected to PCR by using Primer STAR Max (Takara Bio, Dalian, China). Primer sequences for amplifying *SLC7A11* promoter regions that contain the predicted p52-ZER6 binding site were as follows: for the +1310 to +1520 region (primer set 1): 5′-GCA ATT CTC CTG CCT AAG CCT -3′ (forward primer), and 5′- ATG GAA TTT GAG GAC CGG GC-3′ (reverse primer); for the +1230 to +1502 region (primer set 2): 5′-GAC AGA GAC TCG CTC TTT GCC -3′ (forward primer), and 5′- GCG CGG TGG CTC ATA TCT GTA -3′ (reverse primer). Primer sequences for amplifying the +742 to +948 region of *DAZAP1* promoter, which contains the predicted p52-ZER6 binding site were: 5′-CAA AGT GGT AAG GTC GGG AGG -3′ (forward primer); and 5′-GCA GGT CAG GCT CCT ATA GGA -3′ (reverse primer).

2.10. Dual luciferase reporter assay

Cells were seeded into 24-well plates (5×10^4 cells/well). Twenty-four hours later, cells were co-transfected with indicated vectors, reporter vector, and *Renilla* luciferase expression vector (pRL-SV40, Promega, Madison, WI, USA) as internal control. Forty-eight hours later, luciferase activities were measured using the Dual Luciferase Assay System (Promega, Madison, WI, USA). Relative light units of firefly luciferase were normalized to the corresponding *Renilla* luciferase activities. The results are shown as relative to the activities in the corresponding controls, which were assumed as 1.

2.11. In situ hybridization assay

Tissue sections were rehydrated and digested with protease K for 25 min at 37 °C. After pre-hybridization at 37 °C for 1 h, hybridization was carried out by overnight incubation at 37 °C with 8 ng/μL digoxin-conjugated probe specific for the p52-ZER6 isoform (91−113 at the 5′-UTR of *p52-ZER6* mRNA; TCT CGT CTT CGA CCG CAT CCC TC). After being washed with SSC washing buffer at 37 °C, blocking was performed with bovine serum albumin for 30 min. Specifically bound probes were detected by anti-DIG-HRP antibody (Servicebio, Wuhan, China). Nuclei were stained with hematoxylin. Images were taken using Pannoramic Midi (3DHistech, Budapest, Hungary).

2.12. Immunohistochemistry and propidium iodide (PI) staining

Fresh human CRC tissues, normal adjacent tissues, and xenograft tumors were fixed using 4% paraformaldehyde overnight prior to being embedded in paraffin and sectioned at 4 μm thickness using a cryostat. Tissue sections were then incubated with primary antibodies for 1 h followed by incubation with corresponding secondary antibodies conjugated with horse-radish peroxidase or were stained with PI staining (Beyotime Biotechnology, Shanghai, China; final concentration: 4.5 μmol/L) for 10 min. Visualization was performed using a DAB Kit (DAKO, Beijing, China) under the microscope. The nuclei were then counterstained with hematoxylin, followed by dehydration and coverslip mounting. The antibodies used were listed in Supporting Information Table S2. Images were taken using Pannoramic Midi (3DHistech).

2.13. RNA extraction and quantitative reverse transcription-PCR (qRT-PCR)

Cells were prepared as described above. Total RNA was extracted with Trizol (Invitrogen Life Technologies, Carlsbad, CA, USA) according to the manufacturer's instructions. RNA samples were reverse transcribed into cDNA using PrimeScript Reagent Kit with gDNA Eraser (Takara Bio, Dalian, China). qRT-PCR was performed using SYBR Premix ExTaq (Takara Bio, Dalian, China). The sequences of the primers used for qRT-PCR were shown in Table S1. β-Actin was used to normalize sample amplification. The results are shown as relative to the expression level in the corresponding controls, which were assumed as 1.

For xenograft tissues and clinical CRC samples, tissues were frozen in liquid nitrogen and ground before being extracted with Trizol (Invitrogen Life Technologies, Carlsbad, CA, USA). RNA extraction and qRT-PCR were performed as described above.

2.14. Western blotting

Cells were prepared as described above. Protein was extracted using RIPA lysis buffer containing protease inhibitor and phosphatase inhibitor cocktail (complete cocktail; Roche Applied Science, Mannheim, Germany). Protein samples were separated by SDS−PAGE and transferred to PVDF membranes with 0.45 μm pores (Millipore, Billerica, MA, USA). Membranes were then incubated with primary antibodies followed by incubation with corresponding secondary antibodies. Antibodies used were listed in Table S2. Immunoblotting with anti-β-actin antibody was conducted to ensure equal protein loading. Signals were detected by using the SuperSignal West Femto Maximum Sensitivity Substrate detection system (Thermo Scientific, Waltham, MA, USA). Protein quantification was performed using Quantity One software.

For xenograft tissues and clinical CRC samples, tissues were frozen in liquid nitrogen and ground before being lysed with RIPA lysis buffer with protease inhibitor and phosphatase inhibitor cocktail (complete cocktail; Roche Applied Science). Western blotting was performed as described above.

2.15. mRNA degradation analysis and protein degradation analysis

1×10^6 cells were seeded in 6-well plates and treated with actinomycin D (final concentration: 5 μmol/L) or cycloheximide (CHX; final concentration: 30 μg/mL). At the indicated time points, samples were collected and then analyzed *via* qRT-PCR or Western blotting.

2.16. Lipid peroxidation analysis

Cells were prepared as described above before being incubated with 5 μmol/L BODIPY 581/591 C11 (Invitrogen Life Technologies, Carlsbad, CA, USA) in the dark for 20 min at 37 °C. Cells were then harvested by trypsinization, washed twice with PBS, and re-suspended in 200 μL PBS. Fluorescence was analyzed by a flow cytometer equipped with a 488 nm laser for excitation (Beckman Coulter, Inc., CA, USA), and data were collected by the 530 nm band-pass filter.

2.17. GSH and cysteine levels analysis

Cells were prepared as described above, harvested by trypsinization, and collected by centrifugation. The pellets were then dissolved in protein stripping buffer. For xenograft tissues, tissues were homogenized with protein stripping buffer. Intracellular GSH and cysteine levels were then measured using the total GSH assay kit (Beyotime Biotechnology, Shanghai, China) and cysteine assay kit (Solarbio, Beijing, China), respectively. Values were normalized with total protein amount determined using the BCA protein assay kit (Beyotime Biotechnology, Shanghai, China).

2.18. Malondialdehyde (MDA) detection

Cells were prepared as described above, harvested by trypsinization, and collected by centrifugation. The pellets were then dissolved in protein stripping buffer. For xenograft tissues, tissues were homogenized with protein stripping buffer. MDA levels were measured by thiobarbituric acid method using the MDA assay kit (Beyotime Biotechnology, Shanghai, China). The values were normalized with total protein amount determined using the BCA protein assay kit (Beyotime Biotechnology, Shanghai, China).

2.19. Cell death assay

Cells were prepared as described above and re-seeded in 6-well plate at a density of 3×10^5 cells per well. Twenty-four hours later, death cells were stained with PI (Beyotime Biotechnology, Shanghai, China; final concentration: 4.5 μmol/L) and analyzed using flow cytometry (Beckman Coulter, Inc.).

2.20. Cell viability

Cells were prepared as described above before being re-seeded into 96-well plates at a density of 5000 cells/well. Living cells were then counted at indicated time points using colorimetric assay with 3-(4,5-dimethylthiazol-2-yl)-5-(3-carboxymethoxyphenyl)-2-(4-sulfophenyl)-2*H*-tetrazolium (MTS, Promega, Madison, WI, USA) in accordance with the manufacturer's instructions.

2.21. Colony formation assay

Cells were prepared as described above before being re-seeded into 6-well plates at a density of 400 cells/well and cultured for 14 days. Cells were then fixed using 4% paraformaldehyde and stained with crystal violet staining solution (Beyotime Biotechnology, Shanghai, China). Quantification was performed by counting the number of colonies formed. Investigator was blinded during the assessment.

2.22. Statistical analysis

Quantification results were presented as the mean ± standard deviation (SD) ($n = 3$; unless otherwise indicated). Quantification data were analyzed by one-way ANOVA conducted using SPSS Statistics v17.0. (IBM, Chicago, IL, USA). A value of $P < 0.05$ were considered statistically significant.

3. Results

3.1. ZER6 inhibits ferroptosis

To investigate the role of ZER6 in CRC tumorigenesis, we first obtained the clinical data of 814 patients with CRC from 6 GEO datasets (GSE17538, GSE12945, GSE29621, GSE38832, GSE39582, and GSE41258). Subsequently, we conducted prognosis analyses of these patients using the Kaplan−Meier plotter database (http://kmplot.com/analysis/). The results showed that ZER6 expression negatively correlated with overall survival (Fig. 1A). Furthermore, the mRNA and protein expression levels of ZER6 were significantly higher in clinical CRC tissues than in corresponding normal adjacent tissues (Fig. 1B and C). We next investigated the role of ZER6 in CRC cell viability and colony formation potential using two shRNA expression vectors targeting different sites in *ZER6* (Supporting Information Fig. S1A). Knockdown of *ZER6* significantly suppressed its mRNA (Fig. S1B−S1D) and protein (Fig. S1E−S1G) expression levels in $HCT116^{WT}$, HT29, and LoVo cells. It also decreased their viability (Fig. S1H−S1J) and colony formation potential (Fig. S1K−S1M), highlighting the oncogenic role of ZER6.

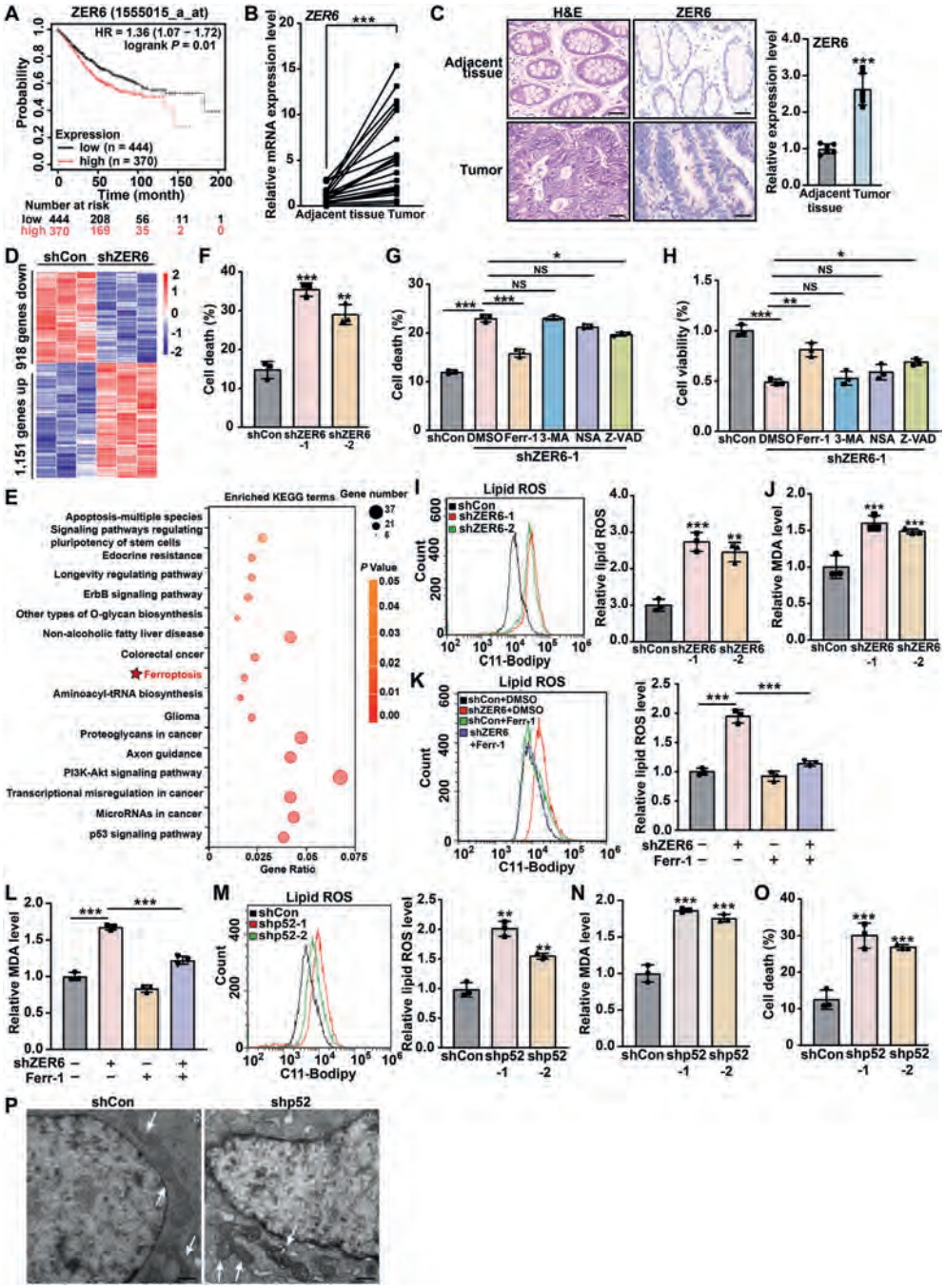

Figure 1 ZER6 positively regulates tumorigenesis by inhibiting ferroptosis. (A) Kaplan−Meier survival plots of clinical CRC patients with either low (black; $n = 444$) or high (red; $n = 370$) ZER6 expression. (B) *ZER6* mRNA expression level in clinical human CRC and corresponding adjacent tissue samples ($n = 22$), as determined by quantitative reverse transcription-PCR (qRT-PCR). (C) Expression levels of ZER6 in clinical human CRC and adjacent tissue samples, as examined by immunohistochemistry staining using serial sections. Representative images (left; scale bar: 50 μm) and quantification results (right; $n = 6$) are shown. (D) Heatmap showing DEGs in *ZER6*-knocked down HCT116^{WT} cells (fold-change ≥1; *P* adj <0.05). (E) Kyoto Encyclopedia of Genes and Genomes analysis of DEGs in *ZER6*-knocked down HCT116^{WT} cells (*P* adj <0.05). (F) Cell death rate of *ZER6*-knocked down HCT116^{WT} cells. (G, H) Cell death rate (G) and relative cell viability (H) of *ZER6*-knocked down HCT116^{WT} cells treated with Ferr-1 (final concentration: 5 μmol/L), 3-MA (final concentration: 10 μmol/L), NSA (final concentration: 5 μmol/L), or Z-VAD (final concentration: 20 μmol/L) for 48 h. (I) Lipid ROS level in *ZER6*-knocked down HCT116^{WT} cells, as assessed by C11-BODIPY staining and flow cytometry. Representative images (left) and quantification results (right) are shown. (J) MDA level in *ZER6*-knocked down HCT116^{WT} cells. (K, L) Lipid ROS (K) and MDA (L) levels in *ZER6*-knocked down HCT116^{WT} cells treated with Ferr-1 (final concentration: 5 μmol/L). (M, N) Lipid ROS (M) and MDA (N) levels in *p52-ZER6*-knocked down HCT116^{WT} cells. (O) Cell death rate of *p52-ZER6*-knocked down HCT116^{WT} cells. (P) Transmission electron microscopy images of mitochondria in *p52-ZER6*-knocked down HCT116^{WT} cells. Arrows: mitochondria; scale bar: 1 μm. Cells transfected with shCon were used as controls. β-Actin was used for qRT-PCR normalization. Quantification data are expressed as mean ± SD ($n = 3$; unless otherwise indicated). *P* values were calculated using one-way ANOVA. $^*P < 0.05$; $^{**}P < 0.01$; $^{***}P < 0.001$; NS: not significant.

To systematically examine the mechanism underlying the oncogenic function of ZER6, we performed RNA-seq-based transcriptome analysis to identify DEGs in *ZER6*-knocked down HCT116^{WT} cells. A total of 2069 DEGs were identified in *ZER6*-knocked down HCT116^{WT} cells, including 1151 upregulated and 918 downregulated genes (Fig. 1D). Kyoto Encyclopedia of Genes and Genomes pathway enrichment analysis revealed DEG enrichment in pathways related to ferroptosis in *ZER6*-knocked down HCT116^{WT} cells (Fig. 1E). We next validated the RNA-seq results by examining the effects of knocking down *ZER6* on various types of cell death. *ZER6* knockdown clearly increased the percentage of PI-positive cells (Fig. 1F), suggesting that ZER6 suppresses cell death. Treatment with the pan-caspase inhibitor Z-VAD slightly suppressed the cell death rate, whereas treatment with the ferroptosis inhibitor Ferr-1 robustly suppressed it (Fig. 1G). Further, Z-VAD slightly recovered the viability of *ZER6*-knocked down HCT116^{WT} cells, whereas Ferr-1 exerted a more significant effect (Fig. 1H). Meanwhile, treatments with the necroptosis inhibitor NSA and autophagy inhibitor 3-MA did not significantly affect the cell death and viability of *ZER6*-knocked down HCT116^{WT} cells. Moreover, *ZER6* knockdown increased lipid ROS and MDA levels, which are characteristics of ferroptosis (Fig. 1I and J), whereas Ferr-1 treatment cancelled these effects (Fig. 1K and L). Taken together, these results suggested that ZER6 suppresses ferroptosis and positively contributes to tumorigenic potential.

To investigate which isoform regulates ferroptosis (Supporting Information Fig. S2A), we constructed shRNA expression vectors to specifically knock down *p52-ZER6* or *p71-ZER6* (Fig. S2B). shp52-ZER6 significantly suppressed the expression of p52-ZER6 in CRC cells at its mRNA (Fig. S2C−S2E) and protein (Fig. S2F−S2H) levels, but did not exert a significant effect on those of p71-ZER6, and *vice versa* (Fig. S2I−S2N). Similarly, overexpression of *p52-ZER6* or *p71-ZER6* did not affect the expression level of the other isoform (Fig. S2O). Together, these results indicate the efficacy and specificity of the vectors used. We next examined the effect of p52-ZER6 on ferroptosis characteristics. *p52-ZER6* knockdown significantly enhanced lipid ROS and MDA levels in HCT116^{WT} cells (Fig. 1M and N), leading to an increase in the cell death rate (Fig. 1O). Similar results were obtained in HT29 and LoVo cells (Supporting Information Fig. S3A−S3D). Moreover, *p52-ZER6* knockdown induced mitochondrial shrinkage, a key event in ferroptosis (Fig. 1P). Intriguingly, *p71-ZER6* knockdown did not have a significant effect on lipid ROS and MDA levels in HCT116^{WT} cells (Fig. S3E and S3F), suggesting that the regulatory function of ZER6 in tumor cell ferroptosis is specific to its p52-ZER6 isoform.

To confirm this, we treated *p52-ZER6*-knocked down HCT116^{WT} cells with Ferr-1, which clearly suppressed lipid ROS levels and cell death induced by *p52-ZER6* knockdown, thereby restoring the viability of *p52-ZER6*-knocked down HCT116^{WT} cells (Fig. S3G−S3I). In contrast, the addition of erastin, a ferroptosis inducer, significantly canceled the effect of *p52-ZER6* overexpression in suppressing lipid ROS and cell death levels, thereby decreasing the viability of HCT116^{WT} cells (Fig. S3J−S3L). Given that HCT116^{WT}, HT29, and LoVo cells are naturally susceptible to ferroptosis (Supporting Information Fig. S4A), we established a HCT116^{EraR} by gradually acclimating the cells to a low-dose erastin for 26 days (Fig. S4B). Compared with HCT116^{WT} cells, HCT116^{EraR} cells demonstrated a less significant increase in lipid ROS and MDA levels as well as cell death rate upon erastin treatment (Fig. S4C−S4E); while the viability of these cells demonstrated the opposite trend (Fig. S4F). Meanwhile, knocking down *p52-ZER6* significantly restored the effect of erastin in inducing lipid ROS and MDA levels, and subsequently, in enhancing the cell death rate and reducing the viability of the HCT116^{EraR} cells. These results further confirmed that p52-ZER6 is crucial for the regulation of CRC cell sensitivity to ferroptosis, and that p52-ZER6 enhances CRC cell viability by suppressing ferroptosis.

3.2. p52-ZER6 suppresses tumor cell ferroptosis by upregulating SLC7A11

To reveal the molecular mechanism through which p52-ZER6 suppresses ferroptosis, we analyzed the fold-changes of ferroptosis-related DEGs in *ZER6*-knocked down HCT116^{WT} cells using the RNA-seq data (Fig. 2A), and validated the results using qRT-PCR. *ZER6*-knockdown most significantly affected the mRNA expression level of *SLC7A11*, encoding a specific light-chain subunit of the cystine/glutamate antiporter (Fig. 2B). This regulatory effect was confirmed in CRC cells (Supporting Information Fig. S5) using another shRNA expression vector targeting a different site in *ZER6*. Consistent with the above finding that p52-ZER6, but not p71-ZER6, can inhibit ferroptosis, only knockdown of *p52-ZER6* significantly suppressed SLC7A11 expression (Fig. 2C−E). Similarly, overexpression of *p52-ZER6*, but not *p71-ZER6*, increased SLC7A11 mRNA and protein expression levels in HCT116^{WT} cells (Fig. 2F−H). The positive correlation between *p52-ZER6* and *SLC7A11* expression was confirmed at the mRNA level in clinical CRC tissues using qRT-PCR (Fig. 2I), and at the protein level by Western blotting (Fig. 2J). This tendency was further confirmed by immunohistochemistry and *in situ* hybridization using serial sections (Fig. 2K). These results showed that both p52-ZER6 and SLC7A11 were highly expressed in CRC tissues compared to normal adjacent tissues (Fig. 2I−K).

SLC7A11 is the core subunit of system X_c^-, which serves as a cystine-glutamate antiporter that mediates the exchange of intracellular glutamate and extracellular cystine. The imported cystine is rapidly reduced to cysteine, which is crucial for *de novo* GSH synthesis[32,33]. Therefore, we next examined whether p52-ZER6 regulates the levels of intracellular cysteine and GSH. Cysteine and GSH levels remarkably decreased in *p52-ZER6*-knockdown HCT116^{WT} cells (Fig. 2L and M), whereas they significantly increased in *p52-ZER6*-overexpressing HCT116^{WT} cells (Fig. 2N and O). Together, these results clearly indicate that p52-ZER6 induces SLC7A11 expression, thereby increasing cystine uptake and *de novo* GSH synthesis.

To confirm the role of SLC7A11 in p52-ZER6-mediated tumor cell ferroptosis resistance, we constructed an *SLC7A11* overexpression vector (Supporting Information Fig. S6A) and shRNA expression vectors targeting *SLC7A11* (Fig. S6B and S6C). *SLC7A11* overexpression significantly restored the levels of cysteine and GSH suppressed in *p52-ZER6*-knocked down HCT116^{WT} cells, suggesting that p52-ZER6 regulation of SLC7A11 expression is crucial for its role in promoting cystine uptake and GSH synthesis (Fig. 3A and B; Fig. S6D). Concomitantly, *SLC7A11* overexpression cancelled the increases in lipid ROS and MDA levels (Fig. 3C and D), and restored mitochondrial morphology in *p52-ZER6*-knocked down HCT116^{WT} cells (Fig. 3E), thereby cancelling the increase in cell death and restoring the viability of *p52-ZER6*-knocked down HCT116^{WT} cells (Fig. 3F and G). In line herewith, knockdown of *SLC7A11*

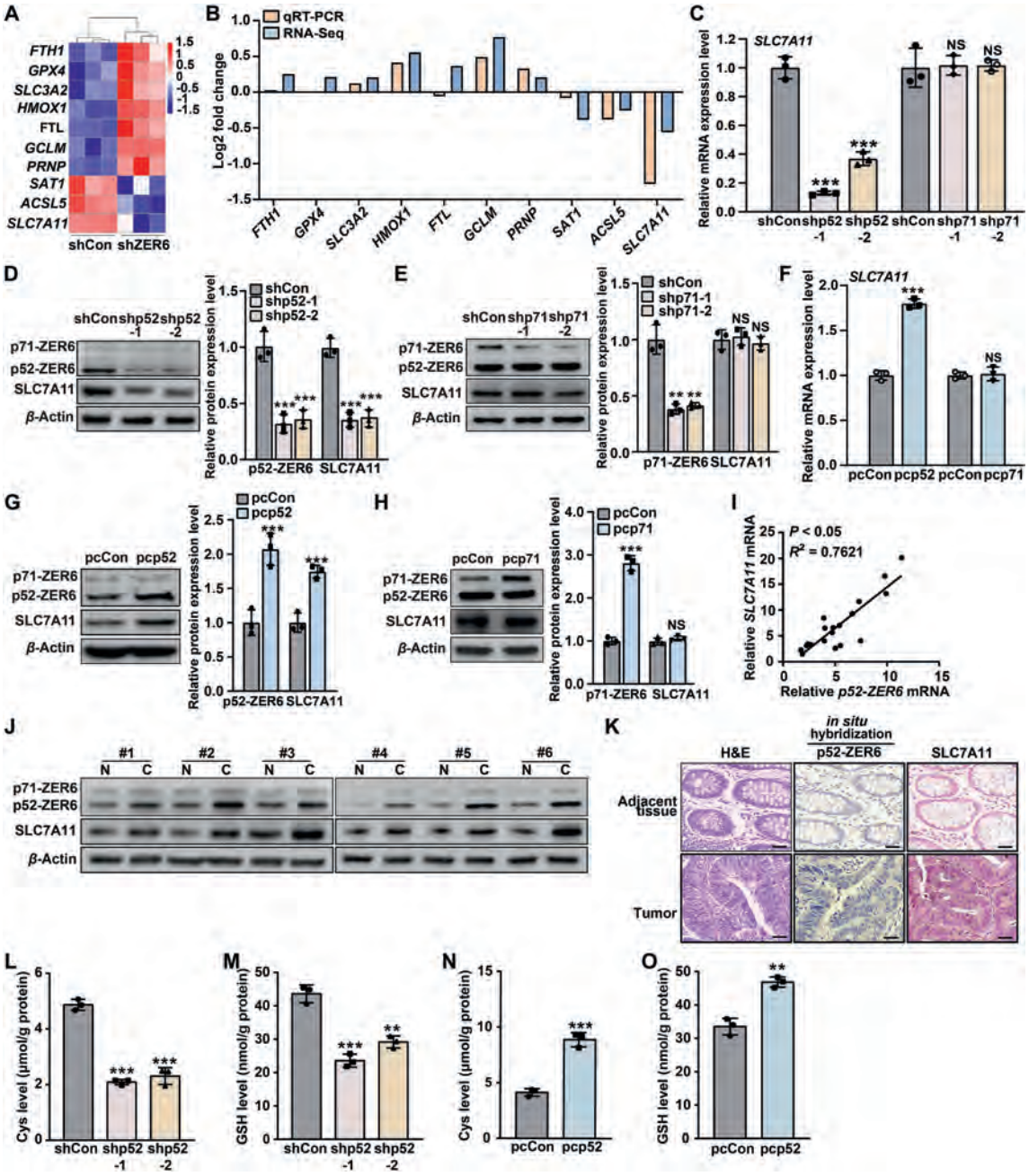

Figure 2 p52-ZER6 promotes SLC7A11 expression. (A, B) Heatmap (A; P adj <0.05; values are scaled as indicated from +1.5 to −1.5) and validation using qRT-PCR (B) of ferroptosis-related DEGs enriched in *ZER6*-knocked down HCT116^{WT} cells. (C) *SLC7A11* mRNA expression level in *p52-ZER6*-knocked down or *p71-ZER6*-knocked down HCT116^{WT} cells, as determined using qRT-PCR. (D, E) SLC7A11 protein expression level in *p52-ZER6*-knocked down (D) or *p71-ZER6*-knocked down (E) HCT116^{WT} cells, as determined using Western blotting. (F) *SLC7A11* mRNA expression level in *p52-ZER6*-overexpressing or *p71-ZER6*-overexpressing HCT116^{WT} cells, as determined using qRT-PCR. (G, H) SLC7A11 protein expression level in *p52-ZER6*-overexpressing (G) or *p71-ZER6*-overexpressing (H) HCT116^{WT} cells, as determined using Western blotting. (I) Correlation between *p52-ZER6* and *SLC7A11* mRNA expression levels in clinical human CRC and corresponding normal adjacent tissues, as determined using qRT-PCR. (J) p52-ZER6 and SLC7A11 protein expression levels in clinical human CRC and corresponding normal adjacent tissue, as determined using Western blotting. (K) p52-ZER6 and SLC7A11 expression levels in clinical human CRC and corresponding normal adjacent tissues, as examined by *in situ* hybridization assay and immunohistochemistry staining using serial sections, respectively (scale bar: 50 μm). (L, M) Cystein (L) and GSH (M) levels in *p52-ZER6*-knocked down HCT116^{WT} cells. (N, O) Cystein (N) and GSH (O) levels in *p52-ZER6*-overexpressing HCT116^{WT} cells. Cells transfected with shCon or pcCon were used as controls. β-Actin was used for qRT-PCR normalization and as Western blotting loading control. Quantification data are expressed as mean ± SD (n = 3). P values were calculated using one-way ANOVA. pcCon: pcEF9-Puro; $^{**}P < 0.01$; $^{***}P < 0.001$; NS: not significant.

canceled the effect of *p52-ZER6* overexpression in promoting cystine uptake and GSH synthesis (Fig. S6E−S6G), thereby increasing lipid ROS and MDA levels suppressed by *p52-ZER6* overexpression (Fig. S6H and S6I). This subsequently cancelled the effects of *p52-ZER6* overexpression in decreasing the cell death rate and increasing cell viability (Fig. S6J and S6K). Together, these findings demonstrate that SLC7A11 is crucial for p52-ZER6-mediated ferroptosis resistance in tumor cells.

Next, to confirm the role of p52-ZER6/SLC7A11 axis in tumorigenesis, we performed xenograft experiments using a *p52-ZER6*-knocked down, *SLC7A11* overexpressing HCT116^{WT} stable cell line (Fig. S6L). It is noteworthy that the mice body weight did not show significant differences among the groups used for xenograft experiments (Fig. S6M). As shown in Fig. 3H, knocking down *p52-ZER6* robustly suppressed the tumorigenic potential of HCT116^{WT} cells, whereas *SLC7A11* overexpression restored it. Western blotting, *in situ* hybridization, and immunohistochemistry staining results confirmed the downregulation of SLC7A11 expression in the xenograft tumors formed by *p52-ZER6*-knocked down HCT116^{WT} cells, as well as the restoration of its expression in those formed by *p52-ZER6*-knocked down, *SLC7A11* overexpressing HCT116^{WT} cells (Fig. 3I and J). Concomitantly, *SLC7A11* overexpression abrogated the effects of *p52-ZER6* knockdown in decreasing intracellular cysteine and GSH levels (Fig. 3K and L), as well as in increasing MDA levels (Fig. 3M) and 4-hydroxynonenal (4-HNE) (Fig. 3N) in the xenograft tumor lesions. Subsequently, our results showed that *SLC7A11* overexpression restored the tumorigenic potential of *p52-ZER6*-knocked down HCT116^{WT} cells by canceling the increase of their cell death rate, as indicated by the decrease in PI-positive cells (Fig. 3O) and restoring their proliferation potential, as indicated by the increase of Ki67-positive cells (Fig. 3N). Thus, these findings demonstrate that the p52-ZER6/SLC7A11 axis was critical for CRC cells tumorigenic potential by promoting ferroposis resistance.

3.3. p52-ZER6 enhances SLC7A11 mRNA stability and tumor cell ferroptosis resistance by promoting DAZAP1 expression

p52-ZER6 is a transcription factor with "GGTGGG" as the core binding sequence[23,26] (Supporting Information Fig. S7A). Prediction using the Eukaryotic Promoter Database (https://epd.expasy.org/epd/) revealed a potential ZER6-binding site in the +1453 to +1458 region of the *SLC7A11* promoter (Fig. S7B). However, reporter assay results using a luciferase reporter vector containing the −127 to +1520 region of the *SLC7A11* promoter (SLC7A11-luc) revealed that neither knockdown nor overexpression of *p52-ZER6* exerted a significant effect on SLC7A11-luc activity (Fig. S7C and S7D). Similar results were obtained in HT29 and LoVo cells (Fig. S7E−S7H), indicating that p52-ZER6 may not regulate *SLC7A11* transcriptional activity. To further confirm this, we performed ChIP assay with two primer sets flanking the predicted binding site to assess whether p52-ZER6 could bind to the *SLC7A11* promoter. Specifically, these primer sets could amplify the +1310 to +1520 and the +1230 to +1502 regions of the *SLC7A11*, producing 210 bp and 272 bp amplicons, respectively. Both primer sets failed to amplify DNA fragment immunoprecipitated using anti-p52-ZER6 antibody, indicating that p52-ZER6 could not bind with *SLC7A11* promoter (Fig. S7I). Intriguingly, in HCT116^{WT} cells treated with CHX which inhibits *de novo* protein synthesis, knocking down of *p52-ZER6* also failed to affect the degradation rate and half-life of SLC7A11 protein, indicating that p52-ZER6 does not regulate its protein stability either (Fig. S7J). These results indicate that p52-ZER6 does not promote SLC7A11 expression *via* transcriptional or post-translational regulation.

Next, we analyzed Gene Ontology term enrichment of the DEGs in *ZER6*-knocked down HCT116^{WT} cells based on the RNA-seq data. The results showed DEG enrichment in "nuclear transcribed mRNA catabolic process", "mRNA catabolic process", "translation factor activity, RNA binding", "mRNA 3′-UTR binding", and "mRNA binding", suggesting that p52-ZER6 may potentially regulate mRNA-binding proteins (Fig. 4A). As RBPs can regulate gene expression through post-transcriptional mechanisms, including mRNA stability[34,35], we next analyzed the effect of *p52-ZER6* knockdown on *SLC7A11* mRNA stability by treating *p52-ZER6*-knocked down HCT116^{WT}, HT29, and LoVo cells with the transcription inhibitor actinomycin D. The half-life of *SLC7A11* mRNA was significantly reduced in *p52-ZER6*-knocked down HCT116^{WT}, HT29, and LoVo cells, suggesting that *p52-ZER6* knockdown accelerated its degradation (Fig. 4B; Supporting Information Fig. S8A and S8B). Meanwhile, *p52-ZER6* overexpression yielded opposite results (Fig. 4C; Fig. S8C and S8D). These results demonstrate that p52-ZER6 promotes SLC7A11 expression most plausibly by stabilizing its mRNA.

To explore which RBPs are involved in regulating *SLC7A11* mRNA stability, we first predicted RBPs that can bind to *SLC7A11* mRNA using RBPmap (http://rbpmap.technion.ac.il/). The results were then compared with the mRNA binding-related DEGs obtained using RNA-seq and ferroptosis-related genes obtained from FerrDbV2 (http://www.zhounan.org/ferrdb/). We found two potential ZER6-regulated RBP candidates: DAZAP1 and ZFP36 (Fig. 4D). Validation using qRT-PCR indicated that the mRNA level of *DAZAP1*, but not that of *ZFP36*, was significantly reduced in *ZER6*-knocked down HCT116^{WT} cells (Fig. 4E). Further analysis revealed that p52-ZER6 positively regulated DAZAP1 mRNA and protein expression levels (Fig. 4F−I). Furthermore, *in situ* hybridization, immunohistochemistry, and Western blotting results showed that both p52-ZER6 and DAZAP1 were upregulated in CRC tissues when compared with those in normal adjacent tissues (Fig. 4J and K). Moreover, correlation analysis using CRC clinical samples showed a positive correlation between *p52-ZER6* and *DAZAP1* mRNA expression in CRC (Fig. 4L). Together, these results suggested the possible regulation of DAZAP1 by p52-ZER6.

To explore whether DAZAP1 is involved in p52-ZER6 regulation of *SLC7A11* mRNA stability, we performed rescue experiments by overexpressing *DAZAP1* in *p52-ZER6*-knocked down HCT116^{WT} cells (Supporting Information Fig. S9A). *DAZAP1* overexpression significantly reduced the SLC7A11 degradation rate in *p52-ZER6*-knocked down HCT116^{WT} cells (Fig. 4M), resulting in the restoration of SLC7A11 mRNA and protein expression levels (Fig. 4N and O). Concomitantly, *DAZAP1* overexpression canceled the effects of *p52-ZER6* knockdown in suppressing cellular cysteine and GSH levels (Fig. S9B and S9C), as well as in increasing lipid ROS and MDA levels (Fig. S9D and S9E), leading to the suppression of cell death and restoration of cell survival in *p52-ZER6*-knocked down HCT116^{WT} cells (Fig. S9F and S9G). Together, these results demonstrate that p52-ZER6 can stabilize SLC7A11 by promoting DAZAP1 expression, thereby promoting p52-ZER6/SLC7A11 axis-mediated tumor cell ferroptosis resistance.

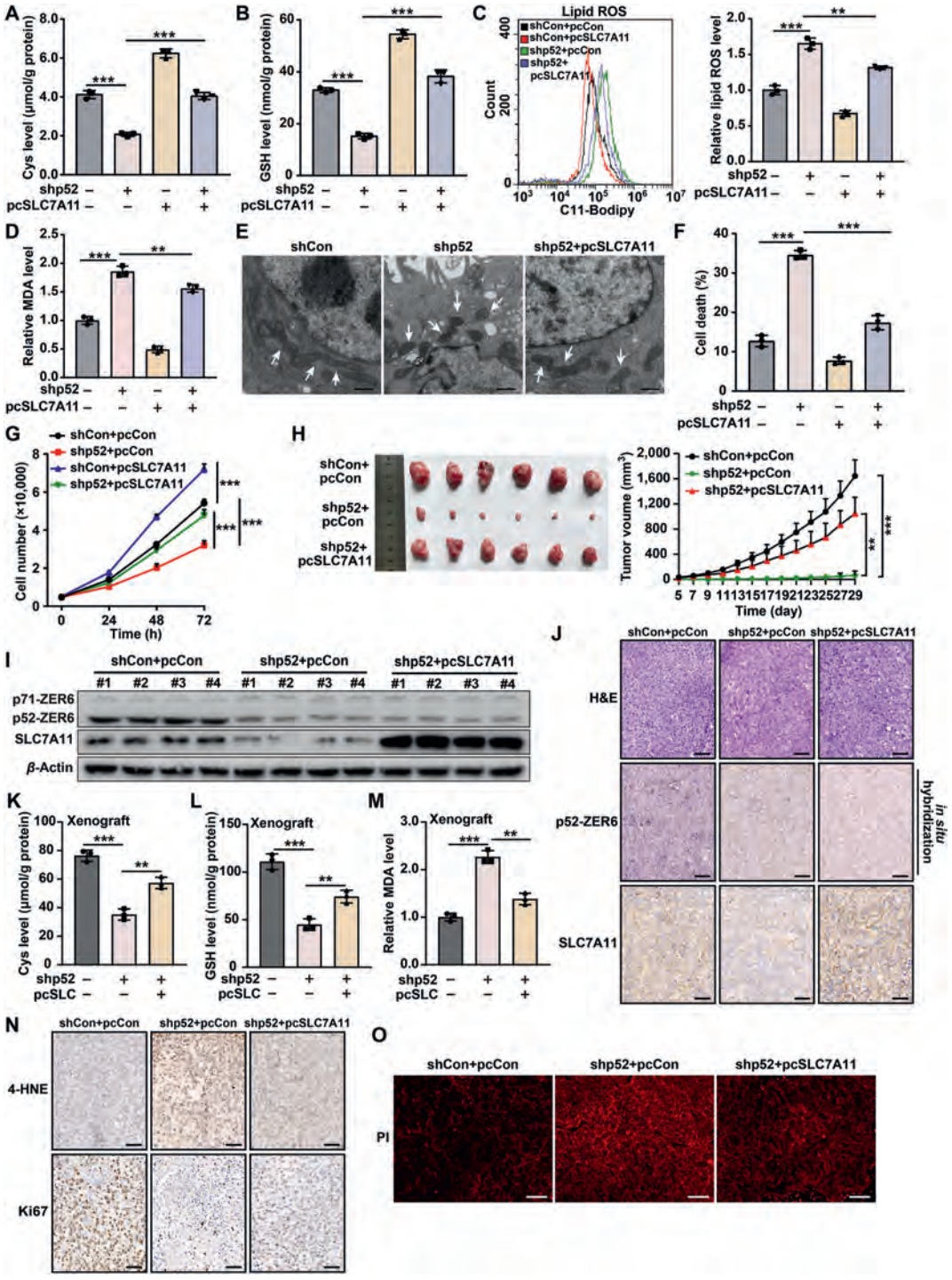

Figure 3 SLC7A11 is crucial for p52-ZER6 regulation on ferroptosis. (A, B) Cysteine (A) and GSH (B) levels in *p52-ZER6*-knocked down, *SLC7A11*-overexpressing HCT116^{WT} cells. (C) Lipid ROS level in *p52-ZER6*-knocked down, *SLC7A11*-overexpressing HCT116^{WT} cells, as assessed by C11-BODIPY staining and flow cytometry. Representative images (left) and quantification results (right; $n = 3$) are shown. (D) MDA level in *p52-ZER6*-knocked down, *SLC7A11*-overexpressing HCT116^{WT} cells. (E) Transmission electron microscopy images of mitochondria in *p52-ZER6*-knocked down, *SLC7A11*-overexpressing HCT116^{WT} cells. Arrows: mitochondria; scale bar: 1 μm. (F, G) Cell death rate (F) and viability (G) of *p52-ZER6*-knocked down, *SLC7A11*-overexpressing HCT116^{WT} cells. (H) Tumorigenic potential of *p52-ZER6*-knocked down, *SLC7A11*-overexpressing HCT116^{WT} stable cells, as examined *in vivo* by subcutaneous injection into BALB/c-*nu*/*nu* mice ($n = 6$). Morphological images of the tumors generated at 29 days after injection (left) and volume of the tumors formed at indicated time points (right) are shown. (I, J) p52-ZER6 and SLC7A11 expression levels in the xenograft tumors formed by HCT116^{WT} cells, as determined using Western blotting (I), as well as *in situ* hybridization and immunohistochemistry staining using serial sections, respectively (J); scale bar: 50 μm. (K–M) Cysteine (K), GSH (L), and MDA (M) levels in the xenograft tumors formed by *p52-ZER6*-knocked down, *SLC7A11*-overexpressing HCT116^{WT} cells. (N) 4-HNE and Ki67 expression levels in the xenograft tumors formed by *p52-ZER6*-knocked down, *SLC7A11*-overexpressing HCT116^{WT} cells,

3.4. *DAZAP1 enhances SLC7A11 mRNA stability by direct binding to its 3′-UTR*

RBPs regulate the stability of their target mRNAs by binding to specific sequences in the target mRNAs *via* their RNA-binding domain[36,37]. A RIP assay using anti-DAZAP1 antibody showed that *SLC7A11* mRNA could be enriched by co-precipitation with DAZAP1, suggesting that DAZAP1 can bind to *SLC7A11* mRNA (Fig. 5A). Prediction using RBPmap (http://rbpmap.technion.ac.il/) revealed 16 potential DAZAP1-binding sites in the 3′-UTR of *SLC7A11* mRNA (Supporting Information Table S3). To determine the specific site in *SLC7A11* mRNA crucial for p52-ZER6/DAZAP1 regulation, we divided the full-length *SLC7A11* mRNA into the following fragments: *SLC7A11*-5′-UTR, *SLC7A11*-CDS, and *SLC7A11*-3′-UTR-1 to *SLC7A11*-3′-UTR-5, comprising the 1 to 1517; 1491 to 3353; 3296 to 4788; 4735 to 6332; and 6325 to 7789 regions of *SLC7A11* 3′-UTR, respectively (Fig. 5B), and constructed corresponding luciferase reporter vectors. Luciferase assays revealed that while knockdown of *p52-ZER6* suppressed the activity of *SLC7A11*-3′-UTR-4, it did not exert a significant effect on *SLC7A11*-5′-UTR, *SLC7A11*-CDS, *SLC7A11*-3′-UTR-1, *SLC7A11*-3′-UTR-2, *SLC7A11*-3′-UTR-3, and *SLC7A11*-3′-UTR-5 activity (Fig. 5C). Similarly, *DAZAP1* overexpression restored the activity of *SLC7A11*-3′-UTR-4, while did not exert any significant effect on that of the other vectors, in *p52-ZER6*-knocked down HCT116^{WT} cells (Fig. 5D). Furthermore, RNA pull-down experiments corroborated that DAZAP1 could only bind to the 4735 to 6332 region of the 3′-UTR of *SLC7A11* mRNA (Fig. 5E).

Next, we further divided the 4735−6332 region into two shorter regions, 4A (4728−5023) and 4B (5110−6332), and performed luciferase assays with corresponding reporter vectors. Although the *p52-ZER6*-knockdown did not affect the activity of *SLC7A11*-3′-UTR-4B, it significantly suppressed that of *SLC7A11*-3′-UTR-4A (Fig. 5F). RNA pull-down experiments revealed that DAZAP1 could only bind to *SLC7A11*-3′-UTR-4A, but not *SLC7A11*-3′-UTR-4B (Fig. 5G). Subsequently, we mutated the UAG sequences to CGA in the two predicted binding sites located within *SLC7A11*-3′-UTR-4A, specifically, at 4828 to 4830, and 4847 to 4849 regions (Fig. 5H). Luciferase reporter assay results showed that the knockdown of *p52-ZER6* did not affect the activity of the Mut-2 vector, harboring the mutation in the 4847 to 4849 region, or that of the Mut-3 vector, encoding the mutation in both the 4828 to 4830, and 4847 to 4849 regions (Fig. 5I). Accordingly, RNA pull-down assays revealed that DAZAP1 could not bind to the *SLC7A11*-3′-UTR fragments with the sequence mutation in the 4847 to 4849 region (Fig. 5J). Together, these results indicate that p52-ZER6 promotes *SLC7A11* mRNA stability most probably *via* DAZAP1, which binds to the 4847 to 4849 region of the 3′-UTR of *SLC7A11* mRNA.

3.5. *p52-ZER6 binds directly to the DAZAP1 promoter and promotes its transcription*

We next explored the molecular mechanism underlying p52-ZER6 regulation of DAZAP1. As shown above, p52-ZER6 regulated the mRNA and protein expression levels of DAZAP1, suggesting a possible regulatory effect of p52-ZER6 on *DAZAP1* transcription. Using the previously reported ZER6-binding motif[23] and the Eukaryotic Promoter Database (https://epd.expasy.org/epd/), we predicted four potential ZER6-binding sites in the *DAZAP1* promoter, and constructed DAZ-luc-1 to DAZ-luc-5 luciferase reporter vectors carrying the −1621 to +1239, −1274 to +1239, +508 to +1239, +741 to +1239, and +867 to +1239 regions of the *DAZAP1* promoter, respectively (Fig. 6A). Luciferase reporter assay results showed that *p52-ZER6*-knockdown significantly suppressed the activities of DAZ-luc-1 to DAZ-luc-4, but not that of DAZ-luc-5, suggesting that the +741 to +866 region of the *DAZAP1* promoter is crucial for p52-ZER6-mediated transcriptional regulation (Fig. 6B).

To determine whether p52-ZER6 can bind directly to the *DAZAP1* promoter at the predicted site, we performed a ChIP assay, confirming the binding of p52-ZER6 to the +742 to +948 region of the *DAZAP1* promoter containing the predicted p52-ZER6-binding site (Fig. 6C). We then constructed a mutant *DAZAP1* promoter luciferase reporter vector, wherein the GGTGGG sequence in the predicted p52-ZER6 core binding site was mutated into TTCTTT (DAZ-luc^{mut}). Knockdown of *p52-ZER6* robustly suppressed the activity of DAZ-luc-4, but not that of DAZ-luc^{mut} (Fig. 6D). Taken together, these results revealed that p52-ZER6 could enhance the transcriptional activity of the *DAZAP1* promoter by directly binding to its +844 to +849 region.

Intriguingly, p71-ZER6 failed to impact the transcriptional activity (Fig. 6E) and expression levels of DAZAP1 (Supporting Information Fig. S10). Given that p71-ZER6 differs from p52-ZER6 in its N terminus, we overexpressed *FLAG-p52*, *FLAG-p71*, and intermediate fragments between p52-ZER6 and p71-ZER6, including FLAG-conjugated p52-ZER6 with an additional 29 amino acids to form a complete KRAB domain (FLAG-p52^{K}) and FLAG-conjugated p52-ZER6 with an additional 138 amino acids to form complete KRAB and HUB-1 domains (FLAG-p52^{KH}) in their N termini (Fig. 6F), and performed ChIP assay using anti-FLAG antibodies. The results showed that only FLAG-p52 and FLAG-p52^{K} could bind directly to the *DAZAP1* promoter (Fig. 6G). Similarly, while *FLAG-p52* and *FLAG-p52^{K}* overexpression significantly induced DAZAP1-luc-1 reporter activity and DAZAP1 expression, *FLAG-p52^{KH}* and *FLAG-p71* overexpression did not (Fig. 6H−J). Together with the above results showing that altering p71-ZER6 expression failed to affect SLC7A11 expression and ferroptotic characteristics, these results indicate that the presence of the HUB-1 domain in p71-ZER6 abrogated its function in promoting *DAZAP1* transcriptional activity and SLCA711 expression, and subsequently, ferroptosis resistance.

3.6. *p52-ZER6 promotes SLC7A11-mediated ferroptosis resistance in a p53-independent manner*

Previous studies have shown that tumor suppressor p53 can induce ferroptosis *via* SLC7A11[38], and that p52-ZER6 can suppress p53 protein accumulation by promoting its ubiquitination/proteasomal degradation[25]. Hence, we next explored whether p52-ZER6 enhances DAZAP1 and SLC7A11 expression levels by regulating

as examined by immunohistochemistry staining using serial sections (scale bar: 50 μm). (O) Cell death rate in the xenograft tumors formed by *p52-ZER6*-knocked down, *SLC7A11*-overexpressing HCT116^{WT} cells, as determined by PI-staining (scale bar: 50 μm). Cells transfected with shCon and/or pcCon were used as controls. β-Actin was used as Western blotting loading control. Quantification data are expressed as mean ± SD ($n = 3$). P values were calculated using one-way ANOVA. pcCon: pcEF9-Puro; $^{**}P < 0.01$; $^{***}P < 0.001$; NS: not significant.

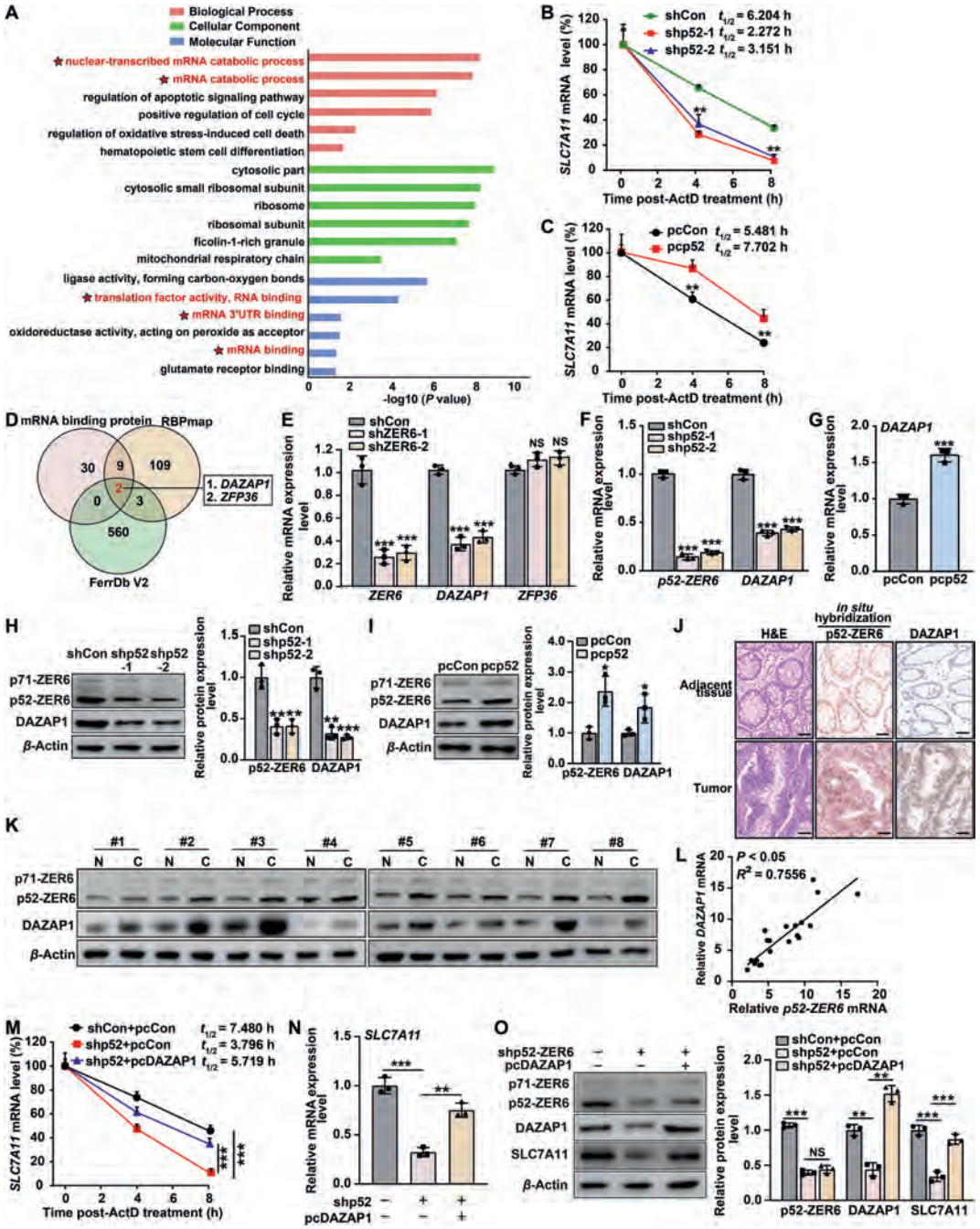

Figure 4 p52-ZER6 enhances *SLC7A11* mRNA stability and CRC cells ferroptotic resistance by promoting DAZAP1 expression. (A) Gene Ontology enrichment analysis of DEGs in *ZER6*-knocked down HCT116^{WT} cells (P adj< 0.05). (B, C) *SLC7A11* mRNA expression levels in *p52-ZER6*-knocked down (B) and *p52-ZER6*-overexpressing (C) HCT116^{WT} cells at indicated time points after actinomycin D treatment, as determined using qRT-PCR. (D) Cross-omics analysis using DEGs in *ZER6*-knocked down HCT116^{WT} cells enriched in "mRNA binding", RBP protein in RBPmap, and ferroptosis-related factor in FerrDb V2. (E) *DAZAP1* and *ZFP36* mRNA expression levels in *ZER6*-knocked down HCT116^{WT} cells, as determined using qRT-PCR. (F, G) *DAZAP1* mRNA expression level in *p52-ZER6*-knocked down (F) and *p52-ZER6*-overexpressing (G) HCT116^{WT} cells, as determined using qRT-PCR. (H, I) DAZAP1 protein expression level in *p52-ZER6*-knocked down (H) and *p52-ZER6*-overexpressing (I) HCT116^{WT} cells, as determined by Western blotting. (J) p52-ZER6 and DAZAP1 expression levels in clinical human CRC and corresponding normal adjacent tissues, as examined by *in situ* hybridization assay and immunohistochemistry staining using serial sections, respectively (scale bar: 50 μm). (K) p52-ZER6 and DAZAP1 protein expression levels in clinical human CRC and corresponding normal adjacent tissues, as determined using Western blotting. (L) Correlation between *p52-ZER6* and *DAZAP1* mRNA expression levels in clinical human CRC and corresponding normal adjacent tissues, as determined using qRT-PCR. (M) *SLC7A11* mRNA expression level in *p52-ZER6*-knocked down, *DAZAP1*-overexpressing HCT116^{WT} cells at indicated time points after actinomycin D treatment, as determined using qRT-PCR. (N, O) SLC7A11 mRNA (N) and protein (O) expression levels in *p52-ZER6*-knocked down, *DAZAP1*-overexpressing HCT116^{WT} cells, as determined using qRT-PCR and Western blotting, respectively. Cells transfected with shCon and/or pcCon were used as controls. β-Actin was

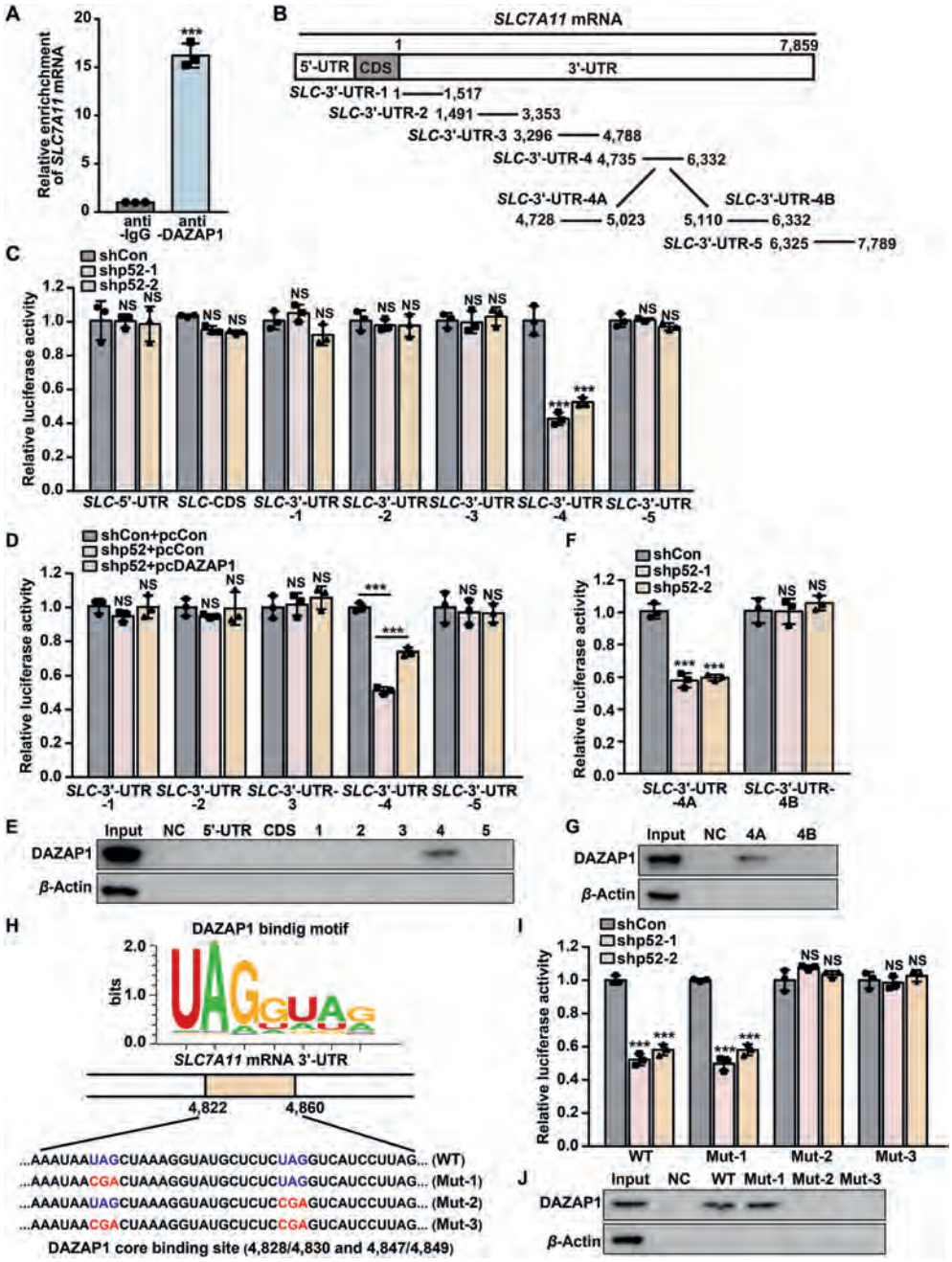

Figure 5 DAZAP1 binds directly to *SLC7A11* 3′-UTR. (A) Binding capacity of DAZAP1 to *SLC7A11* mRNA, as determined by RIP assay using anti-DAZAP1 antibody and qRT-PCR. (B) Schematic diagram of the regions of *SLC7A11* mRNA. (C) Relative luciferase activities of *SLC*-5′-UTR, *SLC*-CDS, and *SLC*-3′-UTR-1 to *SLC*-3′-UTR-5 in *p52-ZER6*-knocked down HCT116^{WT} cells. (D) Relative luciferase activities of *SLC*-3′-UTR-1 to *SLC*-3′-UTR-5 in *p52-ZER6*-knocked down, *DAZAP1* overexpressing HCT116^{WT} cells. (E) Binding capacity of DAZAP1 to *SLC7A11* mRNA regions, as analyzed using RNA pull-down assay. (F) Relative luciferase activities of *SLC*-3′-UTR-4A and *SLC*-3′-UTR-4B in *p52-ZER6*-knocked down HCT116^{WT} cells. (G) Binding capacity of DAZAP1 to *SLC7A11*-3′-UTR-4 regions, as analyzed using RNA pull-down assay. (H) Schematic diagram of mutant SLC7A11-3′-UTR-luc reporter vectors. (I) Relative luciferase activities of mutant SLC7A11-3′-UTR-luc reporter vectors in *p52-ZER6*-knocked down HCT116^{WT} cells. (J) Binding capacity of DAZAP1 to the mutant *SLC7A11*-3′-UTR, as analyzed using RNA pull-down assay. Cells transfected with shCon or pcCon were used as controls. β-Actin was used as Western blotting loading control. Quantification data are expressed as mean ± SD ($n = 3$). *P* values were calculated using one-way ANOVA. pcCon: pcEF9-Puro; ***$P < 0.001$; NS: not significant.

used for qRT-PCR normalization and as Western blotting loading control. Quantification data are expressed as mean ± SD ($n = 3$). *P* values were calculated using one-way ANOVA. pcCon: pcEF9-Puro; ActD: actinomycin D (final concentration: 5 μmol/L); *$P < 0.05$; **$P < 0.01$; ***$P < 0.001$; NS: not significant.

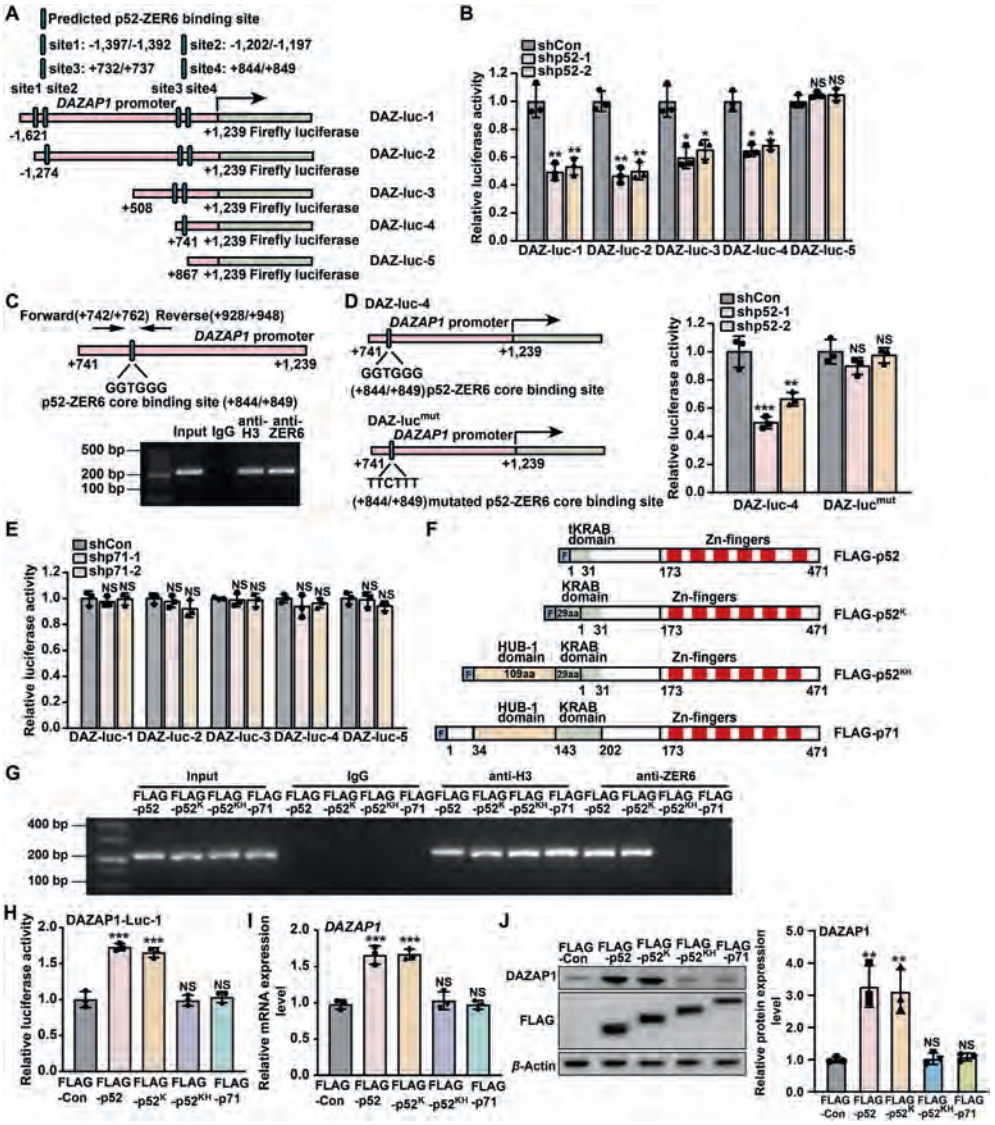

Figure 6 p52-ZER6 promotes *DAZAP1* transcriptional activity by binding directly to its promoter. (A) Schematic diagram of DAZAP1 reporter vectors (DAZ-lucs). (B) Relative luciferase activities of DAZ-luc-1 to DAZ-luc-5 in *p52-ZER6*-knocked down HCT116^{WT} cells. (C) Binding capacity of p52-ZER6 to the predicted region in *DAZAP1* promoter, as examined using ChIP assay with anti-ZER6 antibody followed by PCR. The location of the primer set used for PCR is shown. Anti-histone H3 antibody was used as positive control. (D) Relative luciferase activity of DAZ-luc^{mut} in *p52-ZER6*-knocked down HCT116^{WT} cells. Schematic diagram (left) and luciferase activities (right) are shown. (E) Relative luciferase activities of DAZ-luc-1 to DAZ-luc-5 in *p71-ZER6*-knocked down HCT116^{WT} cells. (F) Schematic diagram of various fragments with intermediate length and sequences between p52-ZER6 and p71-ZER6 conjugated with FLAG. (G) Binding capacities of FLAG-p52, FLAG-p52^{K}, FLAG-p52^{KH}, and FLAG-p71 to the predicted region in the *DAZAP1* promoter, as determined using ChIP assay. (H–J) Relative luciferase activity of DAZ-luc-1 (H), *DAZAP1* mRNA (I), and DAZAP1 protein (J) levels in HCT116^{WT} cells overexpressing *FLAG-p52*, *FLAG-p52^{K}*, *FLAG-p52^{KH}*, or *FLAG-p71*, as determined using qRT-PCR (I) and Western blotting (J), respectively. Cells transfected with shCon or FLAG-Con were used as controls. β-Actin was used for qRT-PCR normalization and as Western blotting loading control. Quantification data are expressed as mean ± SD ($n = 3$). P values were calculated using one-way ANOVA. $^{*}P < 0.05$; $^{**}P < 0.01$; $^{***}P < 0.001$; NS: not significant.

p53. To this extent, we used HCT116^{p53null} cells, which showed a growth advantage compared with HCT116^{WT} cells (Supporting Information Fig. S11A and S11B). Similar to those in HCT116^{WT} cells, knocking down *p52-ZER6* in HCT116^{p53null} cells significantly suppressed the mRNA and protein expression levels of DAZAP1 and SLC7A11 (Fig. 7A and B), whereas *p52-ZER6* overexpression significantly increased them (Fig. S11C and S11D). Suppressing *p52-ZER6* expression did not affect SLC7A11-luc activity, indicating that it did not affect the transcriptional activity of *SLC7A11* (Fig. 7C); however, it significantly shortened the half-life of *SLC7A11* mRNA (Fig. 7D), whereas *p52-ZER6* overexpression clearly prolonged it (Fig. 7E). Together, these results clearly showed that p52-ZER6 could promote *SLC7A11* mRNA stability in a p53-independent manner.

We next examined the effect of altering *p52-ZER6* expression on ferroptosis in HCT116^{p53null} cells. Knockdown of *p52-ZER6* in HCT116^{p53null} cells significantly reduced cellular cysteine and GSH levels (Fig. 7F and G), leading to increases in lipid ROS and

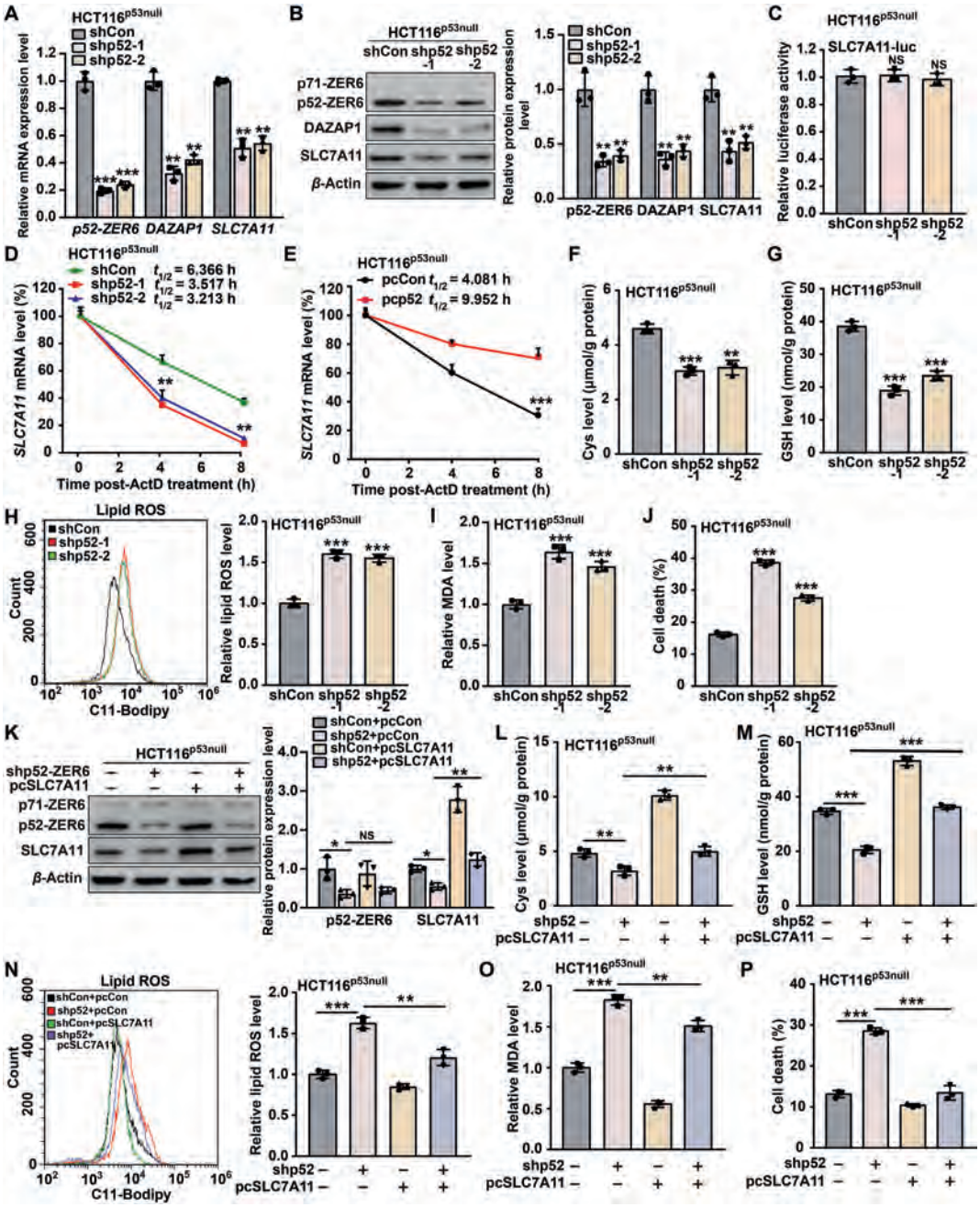

Figure 7 p52-ZER6 suppresses ferroptosis by stabilizing *SLC7A11* mRNA in a p53-independent manner. (A, B) DAZAP1 and SLC7A11 mRNA (A) and protein (B) expression levels in *p52-ZER6*-knocked down HCT116^{p53null} cells, as determined using qRT-PCR and Western blotting, respectively. (C) Relative luciferase activity of SLC7A11-luc in *p52-ZER6*-knocked down HCT116^{p53null} cells. (D, E) *SLC7A11* mRNA expression levels in *p52-ZER6*-knocked down (D) and *p52-ZER6*-overexpressing (E) HCT116^{p53null} cells at indicated time points after actinomycin D treatment, as determined using qRT-PCR. (F, G) Cysteine (F) and GSH (G) levels in *p52-ZER6*-knocked down HCT116^{p53null} cells. (H, I) Lipid ROS (H) and MDA (I) levels in *p52-ZER6*-knocked down HCT116^{p53null} cells. (J) Cell death rate of *p52-ZER6*-knocked down HCT116^{p53null} cells. (K) p52-ZER6 and SLC7A11 protein expression levels in *p52-ZER6*-knocked down, *SLC7A11*-overexpressing HCT116^{p53null} cells, as determined using Western blotting. (L, M) Cysteine (L) and GSH (M) levels in *p52-ZER6*-knocked down, *SLC7A11*-overexpressing HCT116^{p53null} cells. (N, O) Lipid ROS (N) and MDA (O) levels in *p52-ZER6*-knocked down, *SLC7A11*-overexpressing HCT116^{p53null} cells. (P) Cell death rate of *p52-ZER6*-knocked down, *SLC7A11*-overexpressing HCT116^{p53null} Cells. Cells transfected with shCon and/or pcCon were used as controls. *β*-Actin was used for qRT-PCR normalization and as Western blotting loading control. Quantification data are expressed as mean ± SD ($n = 3$). *P* values were calculated using one-way ANOVA. pcCon: pcEF9-Puro; ActD: actinomycin D (final concentration: 5 μmol/L); $^*P < 0.05$; $^{**}P < 0.01$; $^{***}P < 0.001$; NS: not significant.

MDA levels (Fig. 7H and I) and the cell death rate (Fig. 7J). In contrast, *p52-ZER6* overexpression increased the levels of cellular cysteine and GSH in HCT116^{p53null} cells (Fig. S11E and S11F). Hence, p52-ZER6 increases cysteine uptake and GSH production, and eventually suppresses ferroptosis, in a p53-independent manner.

Next, we rescued SLC7A11 expression in *p52-ZER6*-knocked down HCT116^{p53null} cells (Fig. 7K), and analyzed its effect on ferroptosis. *SLC7A11* overexpression clearly restored the cysteine and GSH levels suppressed by *p52-ZER6* knockdown (Fig. 7L and M), thereby cancelling the increases in lipid ROS, MDA, and the cell death rate in *p52-ZER6*-knocked down HCT116^{p53null} cells (Fig. 7N−P). These tendencies were confirmed in *SLC7A11*-knocked down, *p52-ZER6*-overexpressing HCT116^{p53null} cells (Fig. S11G), as *SLC7A11* knockdown abrogated the increases in cysteine uptake and GSH levels mediated by *p52-ZER6* overexpression (Fig. S11H and S11I), leading to the restoration of the MDA level suppressed by *p52-ZER6* in HCT116^{p53null} cells (Fig. S11J). These results suggested that p52-ZER6/SLC7A11 axis can promote tumor cell ferroptosis resistance in the absence of *p53*.

3.7. p52-ZER6/SC7A11 axis promotes tumorigenic potential in a p53-independent manner

Finally, we examined whether p52-ZER6/SLC7A11 axis could regulate tumorigenic potential in a p53-independent manner using xenograft experiments. To this end, we established a *p52-ZER6*-knocked down, *SLC7A11*-overexpressing HCT116^{p53null} stable cell line (Fig. 8A; Supporting Information Fig. S12A), and performed xenograft experiments. While did not significantly affect mice body weight (Fig. S12B), *p52-ZER6* knockdown markedly suppressed the growth of tumors formed by HCT116^{p53null} cells, as shown by tumor morphology on day 22 and tumor volume (Fig. 8B). Meanwhile, *SLC7A11* overexpression abrogated this downregulation effect and restored the tumorigenic potential. Western blotting results showed that SLC7A11 protein expression was suppressed in tumor tissues formed by *p52-ZER6*-knocked down HCT116^{p53null} cells, and, in accordance with their tumorigenic potential, was restored in tumor tissues formed by *p52-ZER6*-knocked down, *SLC7A11*-overexpressing HCT116^{p53null} cells (Fig. 8C). These tendencies were confirmed by *in situ* hybridization and immunohistochemical staining for p52-ZER6 and SLC7A11 using serial sections (Fig. 8D). Moreover, *SLC7A11* overexpression abrogated the effects of knocking down *p52-ZER6* in decreasing the levels of intracellular cysteine and GSH (Fig. 8E and F), as well as in increasing those of MDA and 4-HNE (Fig. 8G and H) in the xenograft tumor lesions. Subsequently, as indicated by the decrease of PI-positive cells (Fig. 8I) and the increase of Ki67-positive cells (Fig. 8H), our results clearly showed that *SLC7A11* overexpression canceled the increase of cell death rate while restoring the proliferation potential of *p52-ZER6*-knocked down HCT116^{p53null} cells suppressed by *p52-ZER*6 knockdown. These results indicate that the p52-ZER6/SLC7A11 signaling axis also plays a crucial role in tumorigenesis by promoting ferroptosis resistance in CRC cells in a p53-independent manner.

In summary, we uncovered an unprecedented link between p52-ZER6 and ferroptosis based on the positive regulation exerted by the p52-ZER6/DAZAP1 axis on *SLC7A11* mRNA stability, which in turn promotes ferroptosis resistance in tumor cells (Fig. 8J).

4. Discussion

Ferroptosis is a unique form of programmed cell death due to lipid peroxide accumulation[39]. Ferroptosis is triggered by aberrant expression of iron accretion-related proteins, such as ferritin light chain 1, ferritin heavy chain 1, and solute carrier family 40 member 1, leading to iron accumulation and subsequently, lipid peroxidation. Defects in lipid peroxide reduction due to aberrant GSH synthesis and GPX4 lead to excessive lipid peroxide accumulation, which finally induces cell death[40]. Ferroptosis resistance, which has been found in various cancers, including hepatocellular carcinoma (HCC), ovarian cancer, CRC, and lung cancer, plays a critical role in promoting tumorigenesis and tumor progression[41-44]. Furthermore, tumor cells exhibit an increased dependence on iron, which promotes the production of ROS, markedly increasing their susceptibility and vulnerability to ferroptosis[45,46]. Hence, targeting tumor cell ferroptosis resistance has attracted attention as an antitumor therapeutic strategy. Indeed, studies have shown that ferroptosis inducers, such as sorafenib and erastin, which target SLC7A11, can improve the efficacy of radiotherapy and chemotherapy, and are thus potential adjuvant treatments for cancer patients[47-49]. In this study, we identified p52-ZER6 as a novel regulator of tumor cell ferroptosis resistance that maintains tumor cell redox homeostasis by promoting the transcription of the RBP *DAZAP1* and stabilizing *SLC7A11* mRNA, providing new insights into the regulatory mechanism of tumor cell redox homeostasis. Although the possible involvement of other cell death forms requires further investigation, our results indicate that p52-ZER6/DAZAP1/SLC7A11 axis-induced ferroptosis resistance plays crucial role in regulating CRC tumorigenesis.

SLC7A11, a specific light-chain subunit of the cystine/glutamate antiporter, contributes to redox homeostasis maintenance as it mediates the cellular uptake of cystine, which, after being reduced to cysteine, forms the cellular reductant GSH[15]. *SLC7A11* overexpression has been observed in various cancers, including bladder[50], ovarian[43], and lung[32] cancers. Previous studies have reported several regulatory mechanisms of *SLC7A11* transcription in tumor cells. *SLC7A11* transcription can be upregulated in tumor cells by imbalanced expression of its transcriptional suppressor, Yin Yang 2, which is downregulated in tumor cells, and its transcriptional activator Yin Yang 1, which is upregulated in tumor cells, or by the inactivation or downregulation of its transcriptional suppressor, p53[30,38]. However, in our study, p52-ZER6 failed to bind to the *SLC7A11* promoter and thus could not regulate its transcriptional activity. Our study revealed the post-transcriptional regulation of *SLC7A11*. We identified the p52-ZER6/DAZAP1 axis as a novel post-transcriptional regulatory pathway of *SLC7A11* that promotes its mRNA stability and expression level, eventually enhancing tumor cell ferroptosis resistance. Hence, this study provided new insights into the regulatory mechanism of SLC7A11, and on GSH synthesis and ferroptosis resistance in tumor cells.

p52-ZER6 upregulation has been observed in various tumors including CRC, breast cancer, and HCC. Further, p52-ZER6 can promote tumorigenic potential by suppressing p53 protein accumulation. However, our knowledge of its biological and pathological functions was limited. The current study revealed that p52-ZER6 upregulation is crucial for tumor cell redox homeostasis and ferroptosis resistance. These findings confirm its role in promoting tumorigenesis and suggest its potential as a target for antitumor therapies. Furthermore, although knocking down *p52-ZER6* exerts

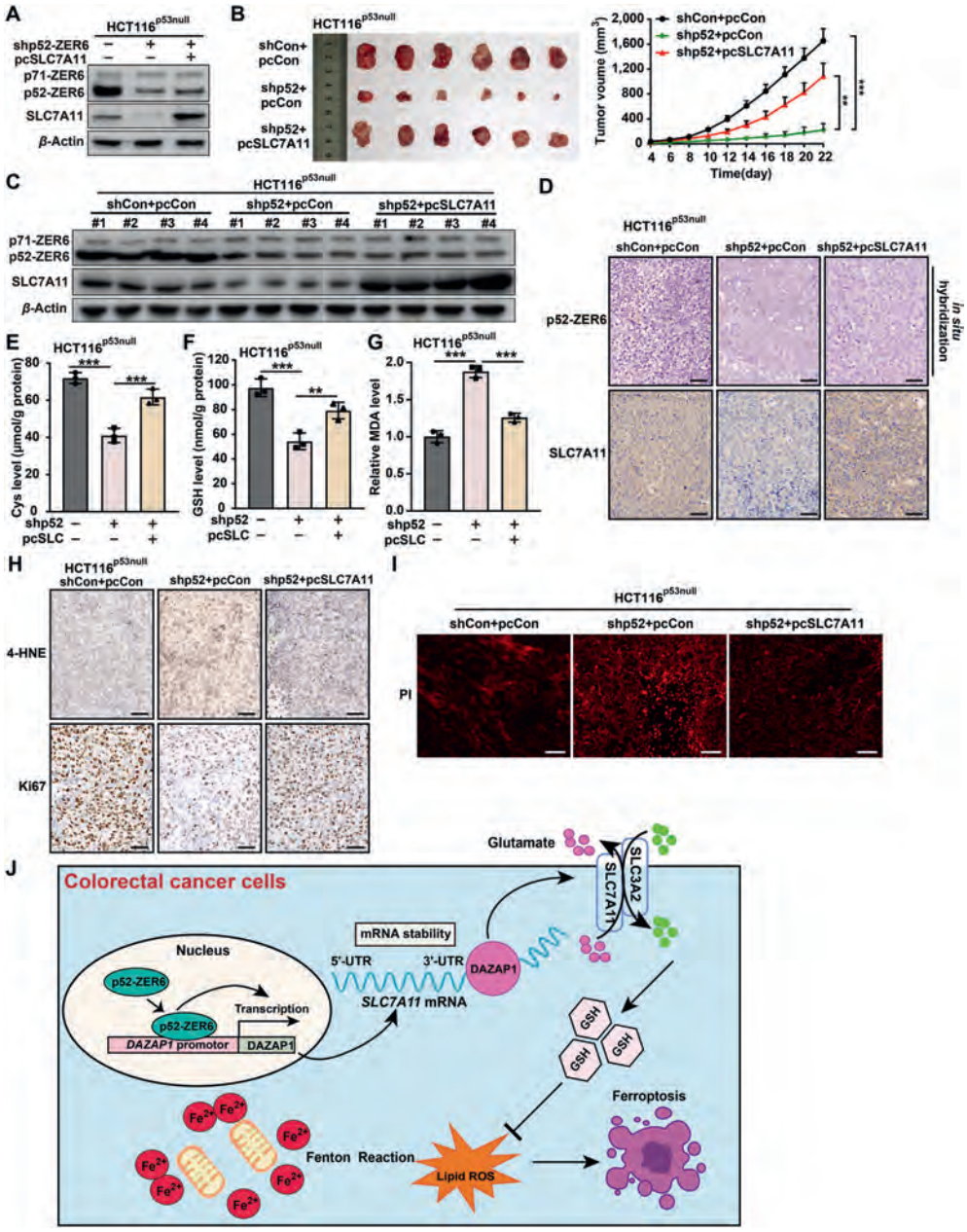

Figure 8 *p52-ZER6* knockdown negatively regulates tumorigenesis by suppressing SLC7A11 in a p53-independent manner. (A) p52-ZER6 and SLC7A11 protein expression levels in *p52-ZER6*-knocked down, *SLC7A11*-overexpressing HCT116^{p53null} stable cells, as determined using Western blotting. (B) Tumorigenic potential of *p52-ZER6*-knocked down, *SLC7A11*-overexpressing HCT116^{p53null} stable cells, as examined *in vivo* by subcutaneous injection into BALB/c-*nu/nu* mice ($n = 6$). Morphological images of the tumors generated at 22 days after injection (left) and the volume of the tumors formed at indicated time points (right) are shown. (C) p52-ZER6 and SLC7A11 protein expression levels in the xenograft tumors formed by HCT116^{p53null} cells, as determined using Western blotting. (D) p52-ZER6 and SLC7A11 in the xenograft tumors formed by *p52-ZER6*-knocked down, *SLC7A11*-overexpressing HCT116^{p53null} cells, as examined by *in situ* hybridization and immunohistochemistry staining using serial sections, respectively (scale bar: 50 μm). (E–G) GSH (E), cysteine (F), and MDA (G) levels in the xenograft tumors formed by *p52-ZER6*-knocked down, *SLC7A11*-overexpressing HCT116^{p53null} cells. (H) 4-HNE and Ki67 expression levels in the xenograft tumors formed by *p52-ZER6*-knocked down, *SLC7A11*-overexpressing HCT116^{p53null} cells, as examined by immunohistochemistry staining using serial sections (scale bar: 50 μm). (I) Cell death rate in the xenograft tumors formed by p52-ZER6-knocked down, SLC7A11-overexpressing HCT116^{p53null} cells, as examined by PI-staining (scale bar: 50 μm). (J) Schematic diagram showing the molecular mechanism of p52-ZER6/DAZAP1 regulation on SLC7A11-mediated tumor cell ferroptosis resistance. Cells transfected with shCon and/or pcCon were used as controls. β-Actin was used as Western blotting loading control. Quantification data are expressed as mean ± SD ($n = 3$, unless otherwise indicated). *P* values were calculated using one-way ANOVA. pcCon: pcEF9-Puro; $^{**}P < 0.01$; $^{***}P < 0.001$.

more significant effect in suppressing SLC7A11 expression and inducing ferroptosis in CRC cells with wild-type *p53*, we revealed that p52-ZER6 regulation of SLC7A11 and ferroptosis occurs irrespective of p53 status. In addition to the existing knowledge that p53 can suppress SLC7A11 expression by blocking its transcription[38] and p52-ZER6 can enhance p53 protein ubiquitination/proteasomal degradation[25], these findings show the presence of both p53-dependent and -independent pathways in p52-ZER6 regulation of SLC7A11, suggesting the possibility of targeting the p52-ZER6/SLC7A11 axis in cancer patients with *p53* deletion and/or loss-of-function mutations, which account for more than 50% of cancer patients.

RBPs can interact with different classes of RNAs, such as mRNAs, tRNAs, as well as non-coding RNAs such as microRNAs (miRNAs), small nuclear RNAs, small nuclear RNAs, and small nucleolar RNAs. RBPs can regulate target gene expression in various post-transcriptional stages, including mRNA alternative splicing, mRNA degradation and stability, mRNA translation, and miRNA processing[51-53]. Hence, RBPs potentially influence various physiological and pathological processes, including embryo development, brain development, muscle development, and particularly, cancer development[28,54-56]. DAZAP1, a proline-rich RBP, was initially identified as a vital binding partner of deleted in azoospermia and deleted in azoospermia-like, and is associated with spermatogenesis and fertility[57]. DAZAP1 regulates its target genes in the post-transcriptional stages, including mRNA stabilization, by binding to its target RNAs[58]. Recent studies reported increased expression of DAZAP1 in tumor tissues, including HCC, multiple myeloma, and seminoma, and its function in regulating tumorigenic potential[59-61]. However, the role of DAZAP1 in promoting tumorigenesis and the regulatory mechanism underlying its increase in tumor tissues was poorly understood. Our study revealed that p52-ZER6 can enhance *DAZAP1* transcription, thereby promoting *SLC7A11* mRNA stability, and subsequently, SLC7A11-mediated ferroptosis resistance and tumor cell redox homeostasis. These results not only elucidate a novel mechanism for the oncogenic function of DAZAP1, but also unravel the molecular mechanism underlying DAZAP1 upregulation in tumor cells.

5. Conclusions

In conclusion, we identified p52-ZER6 as a novel regulator of tumor cell ferroptosis resistance that activates *DAZAP1* transcriptional activity. DAZAP1, in turn, enhances *SLC7A11* mRNA stability by binding to its 3′-UTR, leading to increases in SLC7A11 expression and GSH synthesis, thus promoting ferroptosis resistance. These findings not only provide novel insights into the regulation of ferroptosis, but also uncover new physiological and pathological functions of p52-ZER6. Furthermore, our study suggests a potential strategy to promote the efficacy of ferroptosis-based anti-tumor therapeutics by targeting p52-ZER6.

Acknowledgements

The authors thank Prof. Bert Vogelstein (Johns Hopkins University School of Medicine, USA) for providing HCT116^{p53null} cell lines. This study was financially supported by grants from the National Natural Science Foundation of China (82372655, 82173029, 32270778, and 32070715), and the Natural Science Foundation of Chongqing (CSTB2022NSCQ-MSX0611 and CSTB2022NSCQ-MSX0612, China).

Author contributions

Li Qiu: Writing − review & editing, Writing − original draft, Validation, Project administration, Methodology, Investigation, Formal analysis, Data curation. Wenfang Li: Validation, Software, Methodology, Investigation. Lei Zhang: Visualization, Methodology, Investigation, Formal analysis. Xia Zhang: Investigation, Formal analysis, Conceptualization. Hezhao Zhao: Visualization, Methodology, Conceptualization. Makoto Miyagishi: Methodology, Conceptualization. Shourong Wu: Writing − review & editing, Visualization, Supervision, Resources, Project administration, Methodology, Funding acquisition, Conceptualization. Vivi Kasim: Writing − review & editing, Visualization, Supervision, Resources, Project administration, Investigation, Funding acquisition, Conceptualization.

Conflicts of interest

The authors declare no conflict of interest.

Appendix A. Supporting information

Supporting information to this article can be found online at https://doi.org/10.1016/j.apsb.2025.02.013.

References

1. Hanahan D, Weinberg RA. Hallmarks of cancer: the next generation. *Cell* 2011;**144**:646−74.
2. Tang D, Kang R, Berghe TV, Vandenabeele P, Kroemer G. The molecular machinery of regulated cell death. *Cell Res* 2019;**29**:347−64.
3. Peng F, Liao M, Qin R, Zhu S, Peng C, Fu L, et al. Regulated cell death (RCD) in cancer: key pathways and targeted therapies. *Signal Transduct Target Ther* 2022;**7**:286.
4. Li J, Yi X, Liu L, Wang X, Ai J. Advances in tumor nanotechnology: theragnostic implications in tumors *via* targeting regulated cell death. *Apoptosis* 2023;**28**:1198−215.
5. Tong X, Tang R, Xiao M, Xu J, Wang W, Zhang B, et al. Targeting cell death pathways for cancer therapy: recent developments in necroptosis, pyroptosis, ferroptosis, and cuproptosis research. *J Hematol Oncol* 2022;**15**:174.
6. Koren E, Fuchs Y. Modes of regulated cell death in cancer. *Cancer Discov* 2021;**11**:245−65.
7. Robinson DR, Wu YM, Lonigro RJ, Vats P, Cobain E, Everett J, et al. Integrative clinical genomics of metastatic cancer. *Nature* 2017;**548**:297−303.
8. Niu X, Chen L, Li Y, Hu Z, He F. Ferroptosis, necroptosis, and pyroptosis in the tumor microenvironment: perspectives for immunotherapy of SCLC. *Semin Cancer Biol* 2022;**86**:273−85.
9. Elia I, Haigis MC. Metabolites and the tumour microenvironment: from cellular mechanisms to systemic metabolism. *Nat Metab* 2021;**3**:21−32.
10. Mohammed RN, Khosravi M, Rahman HS, Adili A, Kamali N, Soloshenkov PP, et al. Anastasis: cell recovery mechanisms and potential role in cancer. *Cell Commun Signal* 2022;**20**:81.
11. Mou Y, Wang J, Wu J, He D, Zhang C, Duan C, et al. Ferroptosis, a new form of cell death: opportunities and challenges in cancer. *J Hematol Oncol* 2019;**12**:34.
12. Dixon SJ, Lemberg KM, Lamprecht MR, Skouta R, Zaitsev EM, Gleason CE, et al. Ferroptosis: an iron-dependent form of non-apoptotic cell death. *Cell* 2012;**149**:1060−72.
13. Chen X, Li J, Kang R, Klionsky DJ, Tang D. Ferroptosis: machinery and regulation. *Autophagy* 2021;**17**:2054−81.

14. Chen J, Ye M, Bai J, Hu C, Lu F, Gu D, et al. Novel insights into the interplay between m^6A modification and programmed cell death in cancer. *Int J Biol Sci* 2023;**19**:1748−63.
15. Xie Y, Hou W, Song X, Yu Y, Huang J, Sun X, et al. Ferroptosis: process and function. *Cell Death Differ* 2016;**23**:369−79.
16. Zhang C, Liu X, Jin S, Chen Y, Guo R. Ferroptosis in cancer therapy: a novel approach to reversing drug resistance. *Mol Cancer* 2022;**21**:47.
17. Zhang HC, Deng SH, Pi YN, Guo JN, Xi H, Shi X, et al. Identification and validation in a novel quantification system of ferroptosis patterns for the prediction of prognosis and immunotherapy response in left- and right-sided colon cancer. *Front Immunol* 2022;**13**:855849.
18. Diehn M, Cho RW, Lobo NA, Kalisky T, Dorie MJ, Kulp AN, et al. Association of reactive oxygen species levels and radioresistance in cancer stem cells. *Nature* 2009;**458**:780−3.
19. Yuan L, Li S, Chen Q, Xia T, Luo D, Li L, et al. EBV infection-induced GPX4 promotes chemoresistance and tumor progression in nasopharyngeal carcinoma. *Cell Death Differ* 2022;**29**:1513−27.
20. Ouyang S, Li H, Lou L, Huang Q, Zhang Z, Mo J, et al. Inhibition of STAT3−ferroptosis negative regulatory axis suppresses tumor growth and alleviates chemoresistance in gastric cancer. *Redox Biol* 2022;**52**: 102317.
21. Tsoi J, Robert L, Paraiso K, Galvan C, Sheu KM, Lay J, et al. Multi-stage differentiation defines melanoma subtypes with differential vulnerability to drug-induced iron-dependent oxidative stress. *Cancer Cell* 2018;**33**:890−904.e5.
22. Hangauer MJ, Viswanathan VS, Ryan MJ, Bole D, Eaton JK, Matov A, et al. Drug-tolerant persister cancer cells are vulnerable to GPX4 inhibition. *Nature* 2017;**551**:247−50.
23. Conroy AT, Sharma M, Holtz AE, Wu C, Sun Z, Weigel RJ. A novel zinc finger transcription factor with two isoforms that are differentially repressed by estrogen receptor-alpha. *J Biol Chem* 2002;**277**:9326−34.
24. Stabach PR, Thiyagarajan MM, Weigel RJ. Expression of ZER6 in ERα-positive breast cancer. *J Surg Res* 2005;**126**:86−91; discussion 1-2.
25. Huang C, Wu S, Li W, Herkilini A, Miyagishi M, Zhao H, et al. Zinc-finger protein p52-ZER6 accelerates colorectal cancer cell proliferation and tumour progression through promoting p53 ubiquitination. *EBioMedicine* 2019;**48**:248−63.
26. Tang Y, Li W, Qiu L, Zhang X, Zhang L, Miyagishi M, et al. The p52-ZER6/G6PD axis alters aerobic glycolysis and promotes tumor progression by activating the pentose phosphate pathway. *Oncogenesis* 2023;**12**:17.
27. Li WF, Alfason L, Huang C, Tang Y, Qiu L, Miyagishi M, et al. p52-ZER6: a determinant of tumor cell sensitivity to MDM2-p53 binding inhibitors. *Acta Pharmacol Sin* 2023;**44**:647−60.
28. Qin H, Ni H, Liu Y, Yuan Y, Xi T, Li X, et al. RNA-binding proteins in tumor progression. *J Hematol Oncol* 2020;**13**:90.
29. Gebauer F, Schwarzl T, Valcárcel J, Hentze MW. RNA-binding proteins in human genetic disease. *Nat Rev Genet* 2021;**22**:185−98.
30. Li Y, Li J, Li Z, Wei M, Zhao H, Miyagishi M, et al. Homeostasis imbalance of YY2 and YY1 promotes tumor growth by manipulating ferroptosis. *Adv Sci* 2022;**9**:e2104836.
31. Huang C, Wu S, Ji H, Yan X, Xie Y, Murai S, et al. Identification of XBP1-u as a novel regulator of the MDM2/p53 axis using an shRNA library. *Sci Adv* 2017;**3**:e1701383.
32. Wang X, Chen Y, Wang X, Tian H, Wang Y, Jin J, et al. Stem cell factor SOX2 confers ferroptosis resistance in lung cancer *via* upregulation of SLC7A11. *Cancer Res* 2021;**81**:5217−29.
33. Koppula P, Zhuang L, Gan B. Cystine transporter SLC7A11/xCT in cancer: ferroptosis, nutrient dependency, and cancer therapy. *Protein Cell* 2021;**12**:599−620.
34. Zhang J, Jun Cho S, Chen X. RNPC1, an RNA-binding protein and a target of the p53 family, regulates p63 expression through mRNA stability. *Proc Natl Acad Sci U S A* 2010;**107**:9614−9.
35. Liao WL, Wang WC, Chang WC, Tseng JT. The RNA-binding protein HuR stabilizes cytosolic phospholipase A2α mRNA under interleukin-1β treatment in non-small cell lung cancer A549 Cells. *J Biol Chem* 2011;**286**:35499−508.
36. Xia RM, Liu T, Li WG, Xu XQ. RNA-binding protein RBM24 represses colorectal tumourigenesis by stabilising PTEN mRNA. *Clin Transl Med* 2021;**11**:e383.
37. Van Nostrand EL, Freese P, Pratt GA, Wang X, Wei X, Xiao R, et al. A large-scale binding and functional map of human RNA-binding proteins. *Nature* 2020;**583**:711−9.
38. Jiang L, Kon N, Li T, Wang SJ, Su T, Hibshoosh H, et al. Ferroptosis as a p53-mediated activity during tumour suppression. *Nature* 2015; **520**:57−62.
39. Tang D, Chen X, Kang R, Kroemer G. Ferroptosis: molecular mechanisms and health implications. *Cel Res* 2021;**31**:107−25.
40. Han JX, Luo LL, Wang YC, Miyagishi M, Kasim V, Wu SR. SGLT2 inhibitor empagliflozin promotes revascularization in diabetic mouse hindlimb ischemia by inhibiting ferroptosis. *Acta Pharmacol Sin* 2023;**44**:1161−74.
41. Han L, Huang C, Wang X, Tong D. The RNA-binding protein GRSF1 promotes hepatocarcinogenesis *via* competitively binding to YY1 mRNA with miR-30e-5p. *J Exp Clin Cancer Res* 2022;**41**:17.
42. Zhang W, Sun Y, Bai L, Zhi L, Yang Y, Zhao Q, et al. RBMS1 regulates lung cancer ferroptosis through translational control of SLC7A11. *J Clin Investig* 2021;**131**:e152067.
43. Hong T, Lei G, Chen X, Li H, Zhang X, Wu N, et al. PARP inhibition promotes ferroptosis *via* repressing SLC7A11 and synergizes with ferroptosis inducers in BRCA-proficient ovarian cancer. *Redox Biol* 2021;**42**:101928.
44. Huang P, Duan W, Ruan C, Wang L, Hosea R, Wu Z, et al. NeuroD1−GPX4 signaling leads to ferroptosis resistance in hepatocellular carcinoma. *PLoS Genet* 2023;**19**:e1011098.
45. Floros KV, Cai J, Jacob S, Kurupi R, Fairchild CK, Shende M, et al. MYCN-amplified neuroblastoma is addicted to iron and vulnerable to inhibition of the system Xc-/glutathione axis. *Cancer Res* 2021;**81**: 1896−908.
46. Rodriguez R, Schreiber SL, Conrad M. Persister cancer cells: iron addiction and vulnerability to ferroptosis. *Mol Cell* 2022;**82**:728−40.
47. Dixon SJ, Patel DN, Welsch M, Skouta R, Lee ED, Hayano M, et al. Pharmacological inhibition of cystine−glutamate exchange induces endoplasmic reticulum stress and ferroptosis. *Elife* 2014;**3**:e02523.
48. Lang X, Green MD, Wang W, Yu J, Choi JE, Jiang L, et al. Radiotherapy and immunotherapy promote tumoral lipid oxidation and ferroptosis *via* synergistic repression of SLC7A11. *Cancer Discov* 2019;**9**:1673−85.
49. Ghoochani A, Hsu EC, Aslan M, Rice MA, Nguyen HM, Brooks JD, et al. Ferroptosis inducers are a novel therapeutic approach for advanced prostate cancer. *Cancer Res* 2021;**81**:1583−94.
50. Shen L, Zhang J, Zheng Z, Yang F, Liu S, Wu Y, et al. PHGDH inhibits ferroptosis and promotes malignant progression by upregulating SLC7A11 in bladder cancer. *Int J Biol Sci* 2022;**18**:5459−74.
51. Chatterji P, Rustgi AK. RNA binding proteins in intestinal epithelial biology and colorectal cancer. *Trends Mol Med* 2018;**24**:490−506.
52. Li W, Deng X, Chen J. RNA-binding proteins in regulating mRNA stability and translation: roles and mechanisms in cancer. *Semin Cancer Biol* 2022;**86**:664−77.
53. Eléouët M, Lu C, Zhou Y, Yang P, Ma J, Xu G. Insights on the biological functions and diverse regulation of RNA-binding protein 39 and their implication in human diseases. *Biochim Biophys Acta Gene Regul Mech* 2023;**1866**:194902.
54. Schieweck R, Ninkovic J, Kiebler MA. RNA-binding proteins balance brain function in health and disease. *Physiol Rev* 2021;**101**:1309−70.
55. Zheng S, Zhang X, Odame E, Xu X, Chen Y, Ye J, et al. CircRNA−protein interactions in muscle development and diseases. *Int J Mol Sci* 2021;**22**:3262.
56. Grifone R, Shao M, Saquet A, Shi DL. RNA-binding protein Rbm24 as a multifaceted post-transcriptional regulator of embryonic lineage differentiation and cellular homeostasis. *Cells* 2020;**9**:1891.
57. Smith RW, Anderson RC, Smith JW, Brook M, Richardson WA, Gray NK. DAZAP1, an RNA-binding protein required for development and spermatogenesis, can regulate mRNA translation. *RNA* 2011; **17**:1282−95.

58. Chen Y, Lu Y, Ren Y, Yuan J, Zhang N, Kimball H, et al. Starvation-induced suppression of DAZAP1 by miR-10b integrates splicing control into TSC2-regulated oncogenic autophagy in esophageal squamous cell carcinoma. *Theranostics* 2020;**10**: 4983−96.
59. Deng JJ, Li GP, Lu W, Yan Z, Wang Y. DAZAP1 overexpression promotes growth of HCC cell lines: a primary study using CEUS. *Clin Transl Oncol* 2022;**24**:1168−76.
60. Zhou Y, Huangfu S, Li M, Tang C, Qian J, Guo M, et al. DAZAP1 facilitates the alternative splicing of KITLG to promote multiple myeloma cell proliferation *via* ERK signaling pathway. *Aging (Albany NY)* 2022;**14**:7972−85.
61. Welter H, Herrmann C, Fröhlich T, Flenkenthaler F, Eubler K, Schorle H, et al. Filamin A orchestrates cytoskeletal structure, cell migration and stem cell characteristics in human seminoma TCam-2 cells. *Cells* 2020;**9**:2563.